Summer 8-5-2019

Size Effects in Small Scale Forward Extrusion and Metal Forming

Debabrata Mondal
University of New Orleans, dmondal@uno.edu

Size Effects in Small Scale Forward Extrusion and Metal Forming

A Thesis

Submitted to the Graduate Faculty of the
University of New Orleans
in partial fulfillment of the
requirements for the degree of

Master of Science
in
Engineering
Mechanical

by

Debabrata Mondal

B.S. Bangladesh University of Engineering and Technology, 2015

August, 2019

DEDICATION

To

My Parents

without them I could not come this long way

and

My Siblings

who have been my best friends to guide and support me throughout my life

ACKNOWLEDGEMNT

First of all, I would like to express my deepest gratitude to my advisors, Dr. Paul Schilling and Dr. Paul Herrington. This work would not be possible without their continuous support and directions. I will always be grateful throughout my life for their patience in answering all my questions, both necessary and unnecessary. Their sense of professionalism, enthusiasm, and immense knowledge helped me to strengthen my skills on professional problem-analyzing, problem-solving, and report-writing. I would also like to express my deepest regards to Dr. Uttam Kumar Chakravarty for his valuable thoughts and comments on my research.

I am especially grateful to my colleague, Jeffery Morris for his continuous assistance with hands-on works regarding experiments. I would like to express my gratitude to Mosleh Uddin, M. Shafiqur Rahman, Iftekhar Alam Riyad, Dr. Pratik Sarkar, and Khairul Habib Pulok who have been immensely supportive inside and outside the laboratory. I would like to express my special gratitude to Shovon Sardar and Tushar Mollik, who have been always by my side as true friends which is unforgettable. Finally, I would like to express my sincere appreciation to Kauser Ahmmed Anik and Abdul Motaleb Faysal for their valuable insights and advice regarding python scripting.

Table of Contents

List of Figures

List of Tables

ABSTRACT

Size effects play a significant role in metal processing when the specimen dimensions are reduced. In this study, influence of size effects were investigated on two problem specific processes. First, numerical simulations of a small-scale forward extrusion with varying grain size were performed for both 2D and 3D cases. Here, grains were assigned to non-homogeneous properties in a random fashion. The computational geometry was obtained from Voronoi tessellation in MATLAB, and python-scripting in ABAQUS. Then the effects of size and property non-homogeneity were investigated. Second, a numerical model was simulated to predict final form shapes, punch load requirement, and thickness distribution of hemispherical bowl-shaped forming. The die, punch and cover plate were fabricated using stereolithographic apparatus (SLA). Numerically obtained punch load requirement, thickness distribution, von-Mises contours, and equivalent plastic strain contours were compared for different thickness specimens. Finally, the models were validated by experimental results.

Keywords: size effects, small scale, forward extrusion, non-homogeneous, metal forming, FE modeling.

Chapter 1

Introduction

1.1 Size effects

The so-called size effects play a significant role when the dimensions of a work piece are scaled down to micro scale. Outputs deviate from the conventional predictions with the miniaturization of products. Therefore, investigation of size effects has become essential in microtechnology and nanotechnology. The size effects appear as a set of exceptional characteristics with product miniaturization, and Vollersten [1] categorized them into three kinds, as shown in figure 1.1.

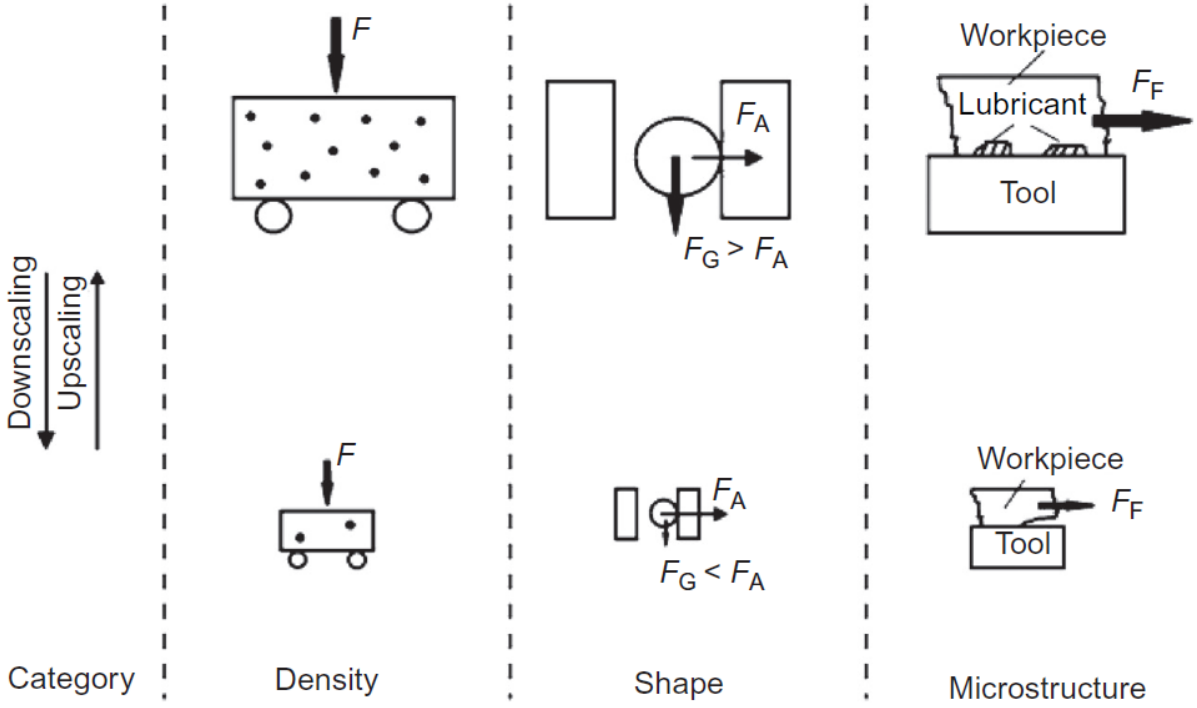

Figure 1.1: Categories of size effects [1]

The three primary categories are density, shape and microstructure size effects. Density size effects demonstrate the inconsistency of a certain feature in a workpiece. For instance, let us consider the black spots in figure 1.1 as a certain type of point defects. As the dimensions of the workpiece are scaled down, the density of the defects may not be the same as before. As a result, material response will be different under the application of load.

The second type - shape size effects - can be understood by an example of a drop of water. As the diameter of the spherical water drop increases, surface area decreases in comparison with the inner volume. Therefore, surface tension force is smaller than the gravity force for a bigger drop of water. However, as the diameter of the water drop decreases, surface area increases relative to inner volume, and hence surface tension force increases and exceeds gravity force. Although the shape of the water drop remains the same (spherical), the resultant of the two opposing forces changes the direction from downward to upward, as the dimensions are scaled down.

Finally, the third type is microstructure size effects. To understand this type, a very common arrangement of tool and workpiece, as shown in figure 1.1 can be considered. Usually lubricants are used at the contact surfaces of tool and workpiece to reduce friction. During the relative motion of workpiece and tool, pockets of lubricants are formed in between the two surfaces. These lubricant pockets can be of two types: open and closed. As the dimensions are reduced, the closed pockets transform to open pockets. Since the behaviors of the closed and open lubricant pockets are not the same, material response changes as the dimensions are scaled down.

However, Liu et al. [2] indicated two major types of size effects that occur during forming processes. These two size effects originate from scaling of geometric size and grain size. The authors investigated geometric and grain size effects separately; the influence of these two size effects were studied on true stress vs strain plots of tensile tests. Geometric size effects on flow stress plots are shown in figure 1.2. Here, the grain size is approximately same but the thickness of the standard tensile specimens varies. As the thickness increased, the flow stress increased. Since stress is a point function, all the plots should have superimposed with one another. However, overlapping of plots was not found due to geometric size effects.

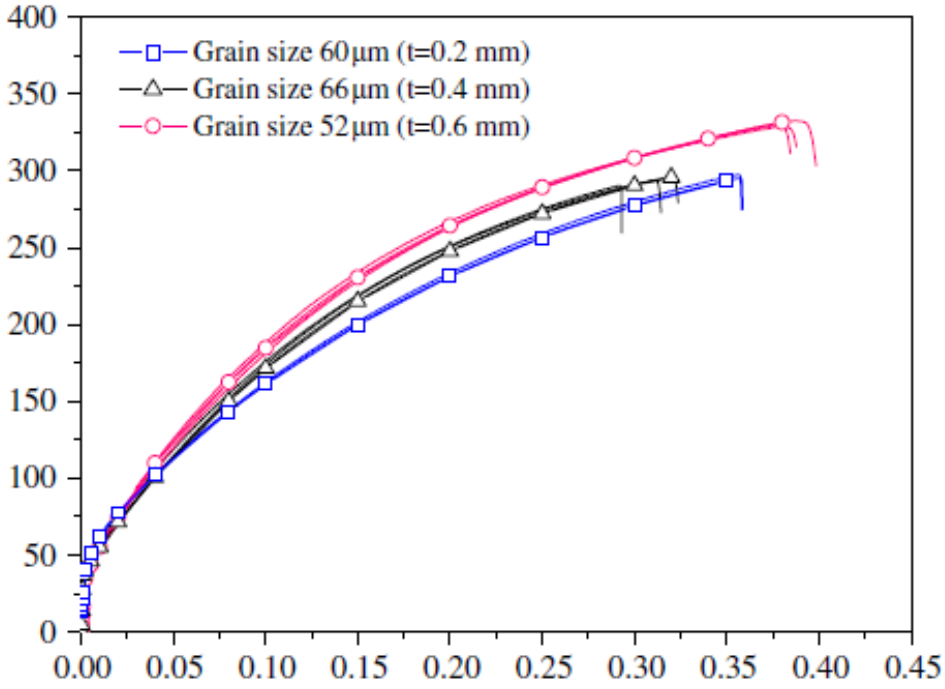

Figure 1.2: Geometric size effects on flow stress plots [2]

Figure 1.3 shows the influence of grain size effects on flow stress curves, obtained from tensile tests. The thickness of the specimen was constant, but grain size was changed. It was found that flow stress increased with the decrease of grain size.

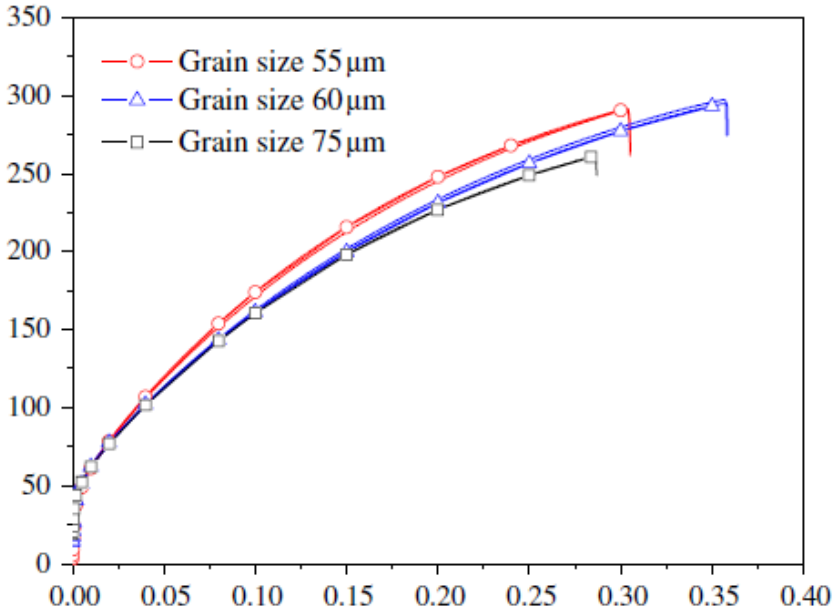

Figure 1.3: Grain size effects on flow stress plots for t = 0.2 mm [2]

It is obvious that size effects are pronounced and sometimes decisive factors to consider in microforming processes. Therefore, study of size effects is essential to determine the issues in problem specific small-scale metal processing.

1.2 Issues due to size effects

Unexpected problems arise in microforming processes due to size effects. These problems are categorized from the aspects of mechanical behavior, tribology, and scatter of material response [3]. When the dimension of a workpiece is large enough, then material is analyzed as bulk material, which means isotropic and homogeneous material properties. However, a metal body possesses numerous grains and each grain has a different orientation and varying mechanical properties. Although these variations are negligible for large scale specimens, these minor differences among the grains become significant as the dimensions are scaled down.

Size effects are significant in metal processing which involves high plastic deformation. Ma et al. [4] investigated the influence of size effects in deep drawing processes on fracture behavior. That study showed an opposing relationship between limiting drawing ratio (LDR) and grain size, i.e., LDR decreases with increase of grain size, and vice versa. Kals and Eckstein [5] studied size effects for problem specific operations, such as tensile tests and air bending of sheet metals on similarity principles by miniaturization. That study showed that, as the thickness of the tensile specimen decreases, flow stress decreases, as shown in figure 1.4. Since surface area increases relative to inner volume as a result of specimen miniaturization, and the surface grains show lower flow stress than the inner grains, thinner tensile specimens show lower flow stress.

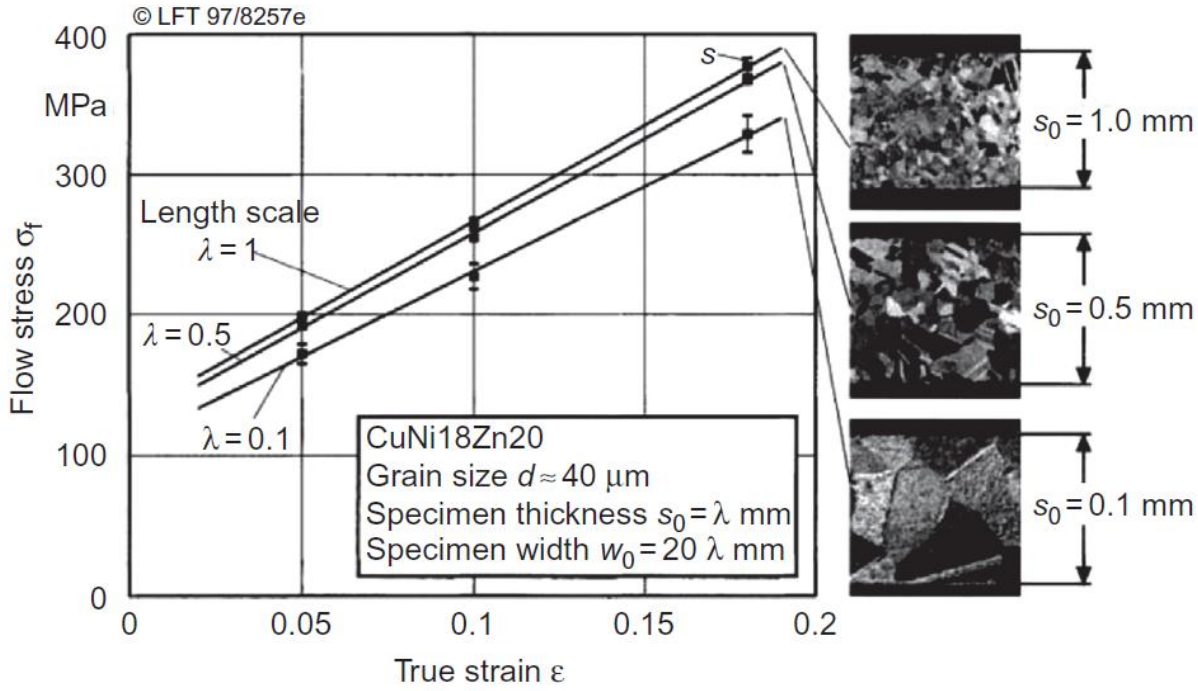

Figure 1.4: Flow curves of CuNi18Zn20 for different values of the length scale λ [5].

Another study was conducted by Li et al. [6] on micro tensile tests of brass foil with different thicknesses for coarse and fine grains. That study showed that samples with finer grains displayed higher flow stress than the samples with coarser grains (figure 1.5).

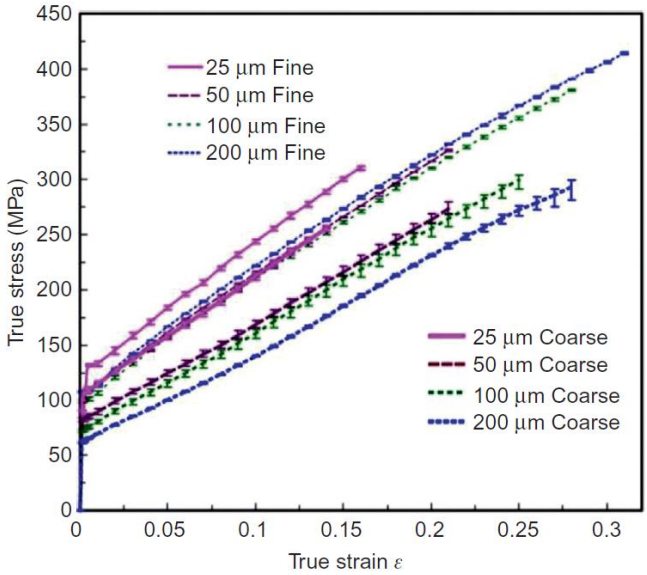

Figure 1.5: Tensile stress-strain curves of CuZn37 brass foils [6].

Moreover, the researchers detected that samples with smaller thickness demonstrated lower elongation before fracture.

Surface finish is a very important requirement for a good quality product, and tribological properties play a significant role on the final shape of parts. One of the major problems due to size effects is related to tribology. Effects of size on friction were investigated by Engel et al. [7]. They conducted scaled ring-test experiments and found that friction increased with product miniaturization. Vollertsen et al. [8] investigated size effects on friction for sheet metal forming processes. That study found that the share of the frictional force in total punch load was greatest for the smallest process dimensions, and vice versa.

With product miniaturization, material response is governed by individual grain properties, since number of grains becomes very low. Scatter of material behavior was studied by Chan et al. [9]. Although the test and environmental conditions and the dimensions of the micro specimens were the same, stress-strain plots did not superimpose with one another, rather they scatter. This happened due to material heterogeneity among the grains. The heterogeneity of the grain properties results from the difference of grain orientation.

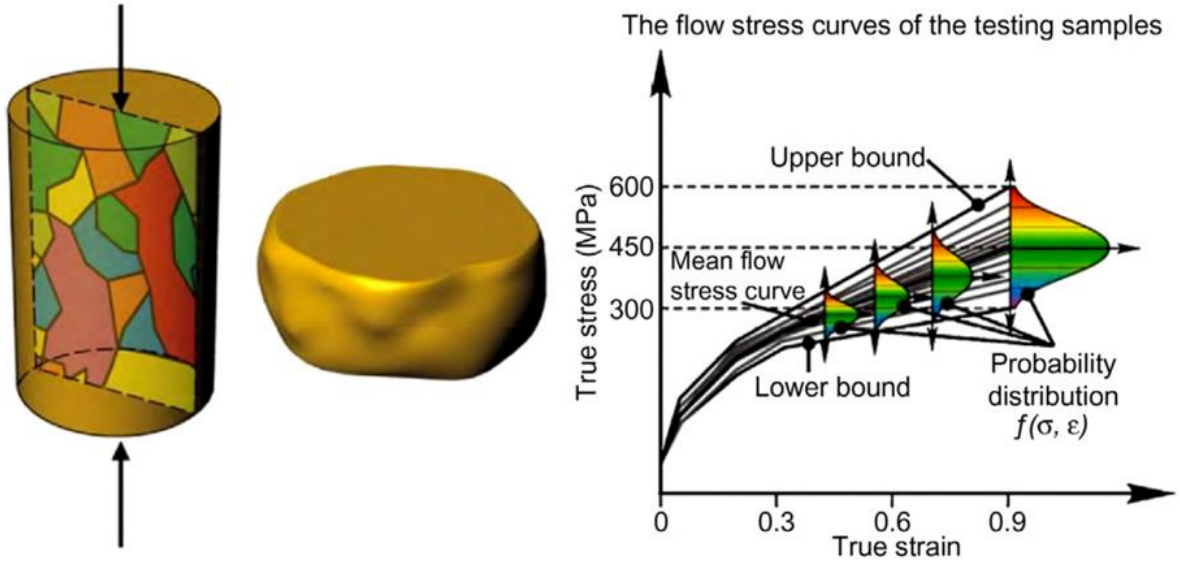

Figure 1.6: Scatter effect with a normal distribution function [9]

The degree of scattering of flow stress was described by the distribution function [9].

$$f(\sigma,\varepsilon)=\frac{1}{S(\varepsilon)\sqrt{2\pi}}e^{-\frac{1}{2}\left[\frac{\sigma(\varepsilon)-\sigma_m(\varepsilon)}{S(\varepsilon)}\right]^2} \tag{1.1}$$

Where σ is the flow stress, ε is the strain, $\sigma(\varepsilon)$ is the flow stress at strain ε, $S(\varepsilon)$ is the standard deviation, and $\sigma_m(\varepsilon)$ is the mean flow stress. The values of $\sigma(\varepsilon)$, $S(\varepsilon)$, and $\sigma_m(\varepsilon)$ can be obtained from the equations (1.2), (1.3), and (1.4), respectively.

$$\sigma(\varepsilon)=\sum_{i=1}^{n}V_i\ \sigma_i(\varepsilon) \tag{1.2}$$

$$S(\varepsilon)=\sqrt{\frac{\sum_{j=1}^{t}\left[\sigma_j(\varepsilon)-\sigma_m(\varepsilon)\right]^2}{t-1}} \tag{1.3}$$

$$\sigma_m(\varepsilon)=\frac{\sum_{j=1}^{t}\sigma_j(\varepsilon)}{t} \tag{1.4}$$

Issues related to mechanical and tribological behavior and material scattering are pronounced when the specimen dimensions are scaled down. These issues significantly affect the final products obtained in small-scale metal processing. Therefore, it is essential to resolve the complication that arises from size effects to ensure the quality of final products.

1.3 Remedies of size effects

Influence of size effects is predominant when products are miniaturized, and some unexpected problems arise. Researchers have been conducting studies to control the influence of size effects on metal processing. Stachowicz et al. [10] conducted a study on warm forming of stainless steel sheet. It was found that with an increase of temperature, a higher value of uniform elongation was achieved. Another strategy of grain refinement can be adopted to mitigate size effects. Parasiz et al. [11] studied grain size effects during microextrusion processes. That study found that for coarser grains, a bending response was observed in forward microextrusion. However, for finer grains, the extruded portion remained straight, as shown on figure 1.7.

Figure 1.7: Samples of pins extruded using the 0.76:0.57 mm die and work pieces having a grain size of 32 microns or 211 microns [11]

From figure 1.7, it is clearly observed that coarser grains create issues in microextrusion. Therefore, grains can be refined to mitigate the problems of bending.

1.4 Research objectives

The goal of this thesis is to predict size effects in two problem specific metal processes. The problem specific metal processes for this study are forward extrusions and sheet metal forming operations at small scales.

Bending response was observed from the experiments of forward micro extrusions for the extruded pins with larger grains [11]. Since performing experiment requires substantial time and investments, computational modeling could be a good tool to predict grain size effects in small-

scale forward extrusions. A Voronoi treated model was implemented in this study to predict grain size effects on 2D small-scale forward extrusions. 2D computational geometry with grains were generated using MATLAB and Python scripting. Afterwards, finite element simulation was performed in the commercial software, ABAQUS/Explicit. Bending magnitude was quantified for each of the specimens with varying grain size. Moreover, punch load requirement was predicted from the model. Similar to 2D model, a 3D finite element model was developed and simulated using the FE software ABAQUS/Explicit. Bending response for forward micro-extrusion was predicted for the specimens with varying grain size. Finally, a case study was accomplished to validate the simulation model.

The second type of problem specific metal forming process — hemispherical bowl-shaped forming—was studied to predict the effect of sheet thickness on the load-displacement response. Computational models were developed and simulated in ABAQUS/Standard to predict punch load, final form shapes, and thickness distribution. Finally, experiments were performed to validate the numerical models.

1.5 Review of literature

Voronoi tessellations are widely used to model geometry consisting of grains to predict the properties of polycrystalline aggregates [14]. A Voronoi tessellation is a structure that consists of cells, which are created from a random array of points. These points are called Poisson points. We can assume that Poisson points initiate the solidification which then uniformly propagates in all directions. The propagation continues until it collides with another one, hence establishing a grain boundary. The geometric grain boundaries are created by inserting lines perpendicular to lines connecting neighboring Poisson points. The details of the Voronoi tessellations can be found in Aurenhammer, 1991 [15] and Okabe et al. [16].

To analyze the process parameters of metal processing at small scales, grain size effects need to be considered. A Voronoi model is used to create a geometry with grains. Researchers studied the influence of size effects on various microforming methods and processes. These processes include micro rolling, micro deep drawing, micro hydromechanical deep drawing, micro bending, micro compression, etc. These studies provide adequate evidence that the Voronoi model with grain heterogeneity can predict the influence of size effects. Cross-wedge rolling failure mechanisms were investigated experimentally by Li et al. [17]. The finite element method was

implemented by Jiang et al. [18] to study cross wedge rolling of metals. The influence of temperature on surface asperity of micro cross wedge rolling was studied and validated by Lu et al. [19]. Considering material heterogeneity, micro flexible rolling was studied by Qu et al. [20]. Process optimization and controlling of material properties in flexible rolling for aluminum alloy sheet were investigated by Engler et al. [21]. Size effects on micro cup drawing was studied by Molotnikov et al. [22]. A Voronoi model was developed for varying grain size and simulated by Luo et al. [23]. To show the dependency of every single grain behavior in small scale forming processes, Wang et al. [24] proposed a multi-region model for simulation. Size dependent FEM-simulation was conducted by Hu et al. [25] for deep drawing of rectangular work pieces. Size effects on cylindrical micro deep drawing was investigated by Ma et al. [26]. A Voronoi blank model was developed and simulated for micro hydro deep drawing of circular caps by Luo et al. [27]. Springback in micro V-bending was studied by Fang et al. [28] considering grain heterogeneity. They used the Voronoi model and compared the simulation result with the experimental result. Influence of grain size effects was investigated by Liu et al. [2] for micro bending using Voronoi tessellation. A simulation of polycrystalline structure with a Voronoi diagram was performed by Fan et al. [29]. Experimental investigation of springback in micro sheet forming for V-bending was conducted by Gau et al. [30]. Voronoi grain based model was developed and simulated by Ghazvinian et al. [31] for brittle rock damage.

Experiments and modeling of anisotropic aluminum extrusions under multi-axial loading were conducted by Dunand et al. [32] and Luo et al. [33]. A rate-independent Taylor-type polycrystalline model was developed and implemented by Guan et al. [34] for single crystals to study the texture development of extruded aluminum tube. A plasticity model was developed by Rousselier et al. [35] for extruded aluminum 6260-T6 at the macroscopic level. Experimental and numerical analysis of the extrusion process for micropins were conducted by Cao et al. [36]. Extrusion texture of a magnesium alloy using crystal plasticity finite element modeling was studied by Shao et al. [37]. The texture development mechanism during the extrusion of magnesium alloy was studied experimentally and numerically by Mayama et al. [38]. Grain size effect on mechanical properties and deformability of titanium alloy was modeled using finite element techniques by Jiang et al. [39] for equal channel angular pressure (ECAP). Effects of grain size and misorientation angle on the deformation of ECAP was studied by Sanusi et al. [40]. Modeling of forward metal extrusion was detailed by Kathirgamanathan et al. [41].

Chapter 2

Mathematical modeling to predict size effects

2.1 Analytical modeling

Liu et al. [2] determined a constitutive model to predict size effects (both grain and geometric) on flow stress of copper alloy tensile specimens.

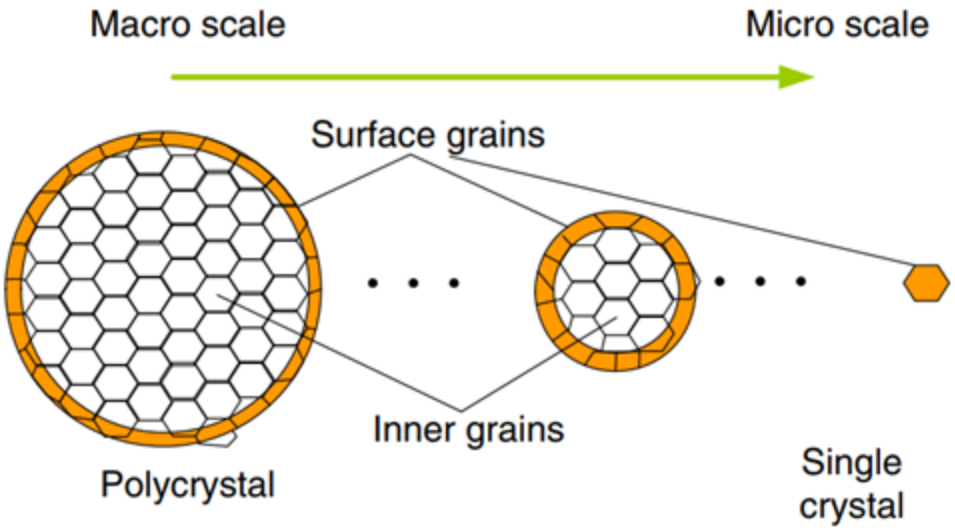

Figure 2.1: Material hierarchy

Let us consider a specimen for analysis. If grains are considered the building blocks, the specimen could be divided into two regions — surface grains and inner grains. When the specimen is under the application of a load, the response of surface grains will not be similar to the response of the inner grains. If the specimen is small enough, then the fraction of the surface grains will be significant enough to consider separately during analysis. The overall flow stress of the specimen

can be expressed in terms of flow stress at the inner portion (σ_{in}) and flow stress in the surface regions (σ_{surf}). Therefore, the overall flow stress can be written as -

$$\sigma = \eta\sigma_{in} + (1-\eta)\sigma_{surf} \tag{2.1}$$

where, η is the fraction of the inner portion.

Now, let us consider a single grain, as shown in the figure 2.2.

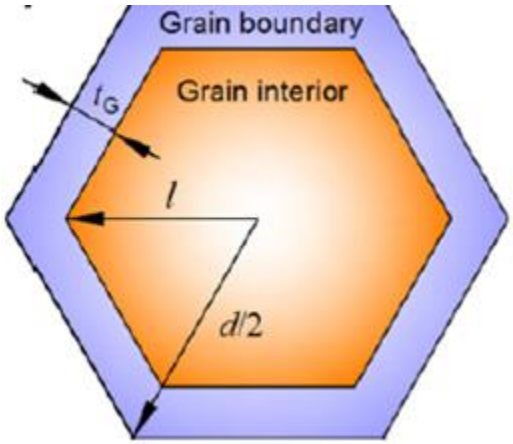

Figure 2.2: Single grain structure

A single grain can be divided into two regions: grain interior and grain boundary. The flow stress in a single grain can be expressed in terms of the flow stress of the grain interior and flow stress at the grain boundary. Therefore, flow stress of single grain can be written as,

$$\sigma_{in} = f_{GI}\sigma_{GI} + f_{GB}\sigma_{GB} \tag{2.2}$$

where, f_{GI} and f_{GB} are the area fractions of the grain interior and grain boundary. They are the functions of average grain size *(d)* and grain boundary thickness *(t_G).* Average grain size and grain boundary thickness are related by an equation [12, 13] as

$$t_G = kd^n \tag{2.3}$$

where t_G and *d* are grain boundary thickness and average grain size, respectively. k, n are constants for specific materials.

Therefore, σ_s is a function of *k, n,* σ_{GB}, σ_{GI}, and *d*.

Now, let us consider the grains at the surface. The response of the surface grains is dominated by grain interior since there is no grain layer on the free surface, i.e., $\sigma_{GI} = \sigma_{surf}$.

For the interior grains, $\sigma_{in} = \sigma_s$

Finally, the equation of overall flow stress can be calculated from the equation (2.4).

$$\sigma = \eta\sigma_s + (1-\eta)\sigma_{GI} \tag{2.4}$$

So, overall flow stress is a function of σ_{GB}, σ_{GI}, k, n, η, and d.

k, n are known constants for specific materials and η is the geometric size factor to represent the fraction of inner portion. σ_{GB}, σ_{GI} are determined from the curve-fitting of more than two stress-strain curves with different size factors.

2.2 Numerical modeling

Forming processes involve high amounts of plastic strain. Due to strain localizing, plastic damage, nonlinearity, and inhomogeneous stress-strain fields, analytical models fail to predict size effects in micro-forming processes. Therefore, numerical modeling is used to predict the response in small-scale forming processes. Finite element (FE) modeling is used to analyze the deformation and process parameters in forming processes; researchers adopted a number of different models to predict size effects. Two very well-known approaches for microforming processes are crystal plasticity finite element modeling (CPFEM), and finite element simulation of a Voronoi model.

2.2.1 Crystal plasticity finite element modeling (CPFEM)

CPFEM is performed based on the crystal plasticity (CP) theory. The geometrics and kinematics of crystal plastic deformation are described in references [42-47]. The basic equations of CP kinematics are described below.

$$Gross\ deformation\ gradient, \boldsymbol{F} = \frac{\partial x}{\partial X} = \boldsymbol{F}^* \cdot \boldsymbol{F}^p \tag{2.5}$$

Superscripts * and p indicate elastic and plastic, respectively.

$$Slip\ vector, \boldsymbol{s}^*_{(\alpha)} = \boldsymbol{F}^* \cdot \boldsymbol{s}_{(\alpha)} \tag{2.6}$$

$$Undeformed\ normal\ vector, \boldsymbol{m}^*_{(\alpha)} = \boldsymbol{m}_{(\alpha)} \cdot \boldsymbol{F}^{*-1} \tag{2.7}$$

$$Current\ velocity\ gradient, \boldsymbol{L} = \frac{\partial v}{\partial x} = \frac{\partial v}{\partial X} \cdot \frac{\partial X}{\partial x} = \dot{\boldsymbol{F}} \cdot \boldsymbol{F}^{-1} = \boldsymbol{L}^* + \boldsymbol{L}^p \tag{2.8}$$

$$\boldsymbol{L}^* + \boldsymbol{L}^p = \dot{\boldsymbol{F}}^* \cdot \boldsymbol{F}^{*-1} + \boldsymbol{F}^* \cdot \dot{\boldsymbol{F}}^p \cdot \boldsymbol{F}^{p-1} \cdot \boldsymbol{F}^{*-1} \tag{2.9}$$

Plastic deformation in single crystal:

$$\boldsymbol{F}^p = \boldsymbol{I} + \gamma_{(\alpha)} \boldsymbol{s}_{(\alpha)} \otimes \boldsymbol{m}_{(\alpha)} \tag{2.10}$$

$$\dot{\boldsymbol{F}}^p = \sum_{\alpha=1}^{n} \dot{\gamma}_{(\alpha)} \boldsymbol{s}_{(\alpha)} \otimes \boldsymbol{m}_{(\alpha)} \tag{2.11}$$

$$\boldsymbol{F}^{p-1} = \boldsymbol{I} - \sum_{\alpha=1}^{n} \gamma_{(\alpha)} \boldsymbol{s}_{(\alpha)} \otimes \boldsymbol{m}_{(\alpha)} \tag{2.12}$$

$$\dot{\boldsymbol{F}}^p \cdot \boldsymbol{F}^{p-1} = \sum_{\alpha=1}^{n} \dot{\gamma}_{(\alpha)} \boldsymbol{s}_{(\alpha)} \otimes \boldsymbol{m}_{(\alpha)} \tag{2.13}$$

$\gamma_{(\alpha)}$ is the shear strain and $\dot{\gamma}_{(\alpha)}$is the shear rate.

$$\boldsymbol{L}^* = \dot{\boldsymbol{F}}^* \cdot \boldsymbol{F}^{*-1} \tag{2.14}$$

$$\boldsymbol{L}^p = \boldsymbol{F}^* \cdot \dot{\boldsymbol{F}}^p \cdot \boldsymbol{F}^{p-1} \cdot \boldsymbol{F}^{*-1} = \sum_{\alpha=1}^{n} \dot{\gamma}_{(\alpha)} \boldsymbol{s}^*{}_{(\alpha)} \otimes \boldsymbol{m}^*{}_{(\alpha)} \tag{2.15}$$

$$\boldsymbol{L} = \boldsymbol{D} + \boldsymbol{\Omega} \tag{2.16}$$

$\boldsymbol{D}$ *and* $\boldsymbol{\Omega}$ are symmetric tensors of deforming velocity and rotating velocity, respectively.

$$D_{ij} = \frac{1}{2}\left(\frac{\partial v_i}{\partial x_j} + \frac{\partial v_j}{\partial x_i}\right) \tag{2.17}$$

$$\Omega_{ij} = \frac{1}{2}\left(\frac{\partial v_i}{\partial x_j} - \frac{\partial v_j}{\partial x_i}\right) \tag{2.18}$$

$$\boldsymbol{D} = \boldsymbol{D}^* + \boldsymbol{D}^p, \boldsymbol{\Omega} = \boldsymbol{\Omega}^* + \boldsymbol{\Omega}^p \tag{2.19}$$

$$\boldsymbol{D}^p + \boldsymbol{\Omega}^p = \boldsymbol{F}^* \cdot \dot{\boldsymbol{F}}^p \cdot \boldsymbol{F}^{p-1} \cdot \boldsymbol{F}^{*-1} \tag{2.20}$$

$$\boldsymbol{D}^p + \boldsymbol{\Omega}^p = \sum_{\alpha=1}^{n} \dot{\gamma}_{(\alpha)} \boldsymbol{s}^*{}_{(\alpha)} \otimes \boldsymbol{m}^*{}_{(\alpha)} \tag{2.21}$$

$$\dot{\boldsymbol{F}}^p \boldsymbol{F}^{p-1} = \sum_{\alpha=1}^{n} \dot{\gamma}_{(\alpha)} \boldsymbol{s}_{(\alpha)} \boldsymbol{m}_{(\alpha)} \tag{2.22}$$

The User-defined Material Mechanical Behavior (UMAT) is an interface for FORTRAN program by which a problem can be simulated in ABAQUS using CP theory, since CP is not a built in code in ABAQUS.

2.2.2 Voronoi model with grain heterogeneity

The first step is to obtain a Voronoi tessellation with grains. The Voronoi algorithm is used to generate the geometry. After that the grains are assigned non-homogeneous grain properties. Then under the application of load, applying boundary conditions, the simulation is performed. Some of the features of Voronoi model with grain heterogeneity simulation are stated below.

1. Resulting anisotropy is assigned to grains instead of grain orientation.
2. Computational cost and time requirement are lower than CPFEM.
3. Model assumes every single grain as homogeneous and isotropic.
4. Empirical statistical distribution function is required to obtain material heterogeneity.

The details of Voronoi model simulation for small-scale forward extrusion will be described in chapters 3 and 4. Implementation of 2D Voronoi model simulation will be elaborated in chapter 2, and 3D Voronoi model simulation will be described in chapter 4.

Chapter 3

2D modeling: predicting grain size effects on forward extrusion

In this chapter, effects of grain size will be discussed on small scale forward extrusion, as shown in figure 3.1. A billet was placed inside the die-cavity before the extrusion operation. Then a punch was used to cause material flow through the die opening. The die opening had a smaller lateral dimension than the die-cavity. As the punch moves down, extrusion occurs and hence the dimensions of the billet change. Simulations were performed using a 2D Voronoi model with grain heterogeneity.

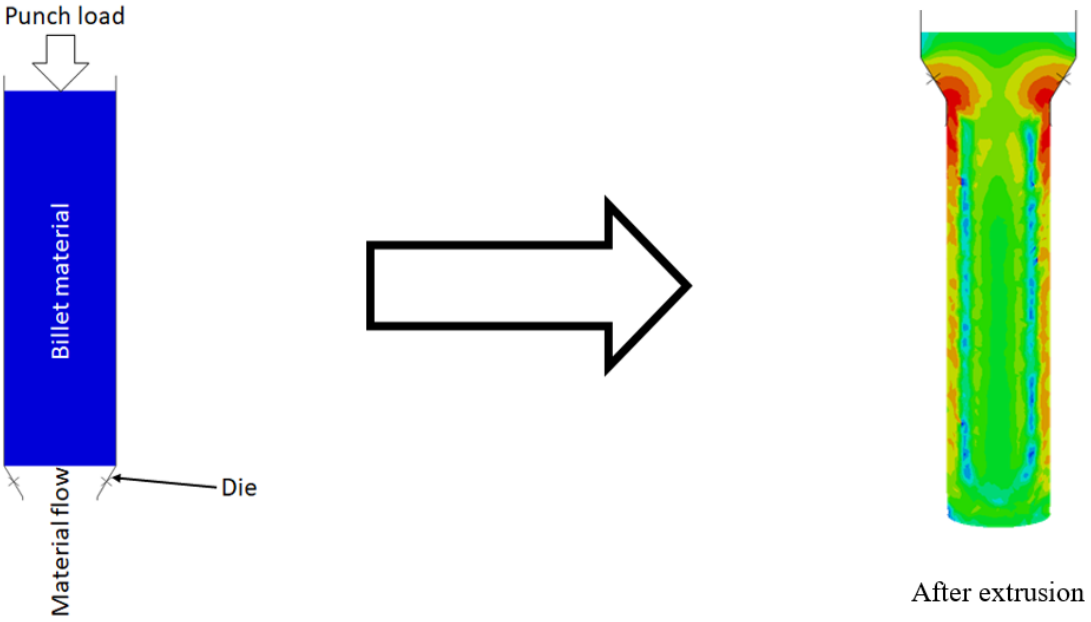

Figure 3.1: Forward extrusion

3.1 Problem statement

Numerical simulations of forward extrusion were conducted for an aluminum alloy with grain sizes of 291, 325, and 420 microns. In the 2-D model, the billet was of length 12 mm and width of 3 mm. The die was considered as perfectly rigid body with a die angle of 26.6º with the vertical line. The billet width was reduced to 2 mm, i.e., a 33.33% decrease along the lateral dimension. The schematic is shown in the figure 3.2.

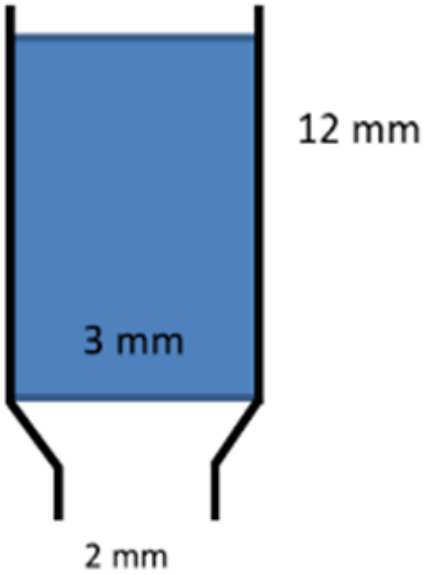

Figure 3.2: Schematic of the billet-die assembly

3.2 Material properties

For the Voronoi modeling with grain heterogeneity, experimental data for the plastic behavior of the extruded material are needed. The billet material was aluminum; the material properties were obtained from the metal handbook [48]. The general properties are given below:

Density = 2672 kg/m^3

Elastic Modulus, E = 70 GPa

Poisson's ratio = 0.33

To determine the effect of material heterogeneity, four sets of plastic properties (stress vs strain) were calculated by offsetting ±20% and ±40% of the experimental data, as shown in figure in 3.3. The plot with legend "Avg" indicates average stress-strain plot for the billet material. This curve was calculated from the tensile test of bulk aluminum specimens. In practice, the stress values are not available at higher amount of strains. Therefore, well-known Ramberg-Osgood equations were used to avail the stress values at higher strains. The stress values at higher strains are necessary because the extrusion process involves higher amount of plastic deformation.

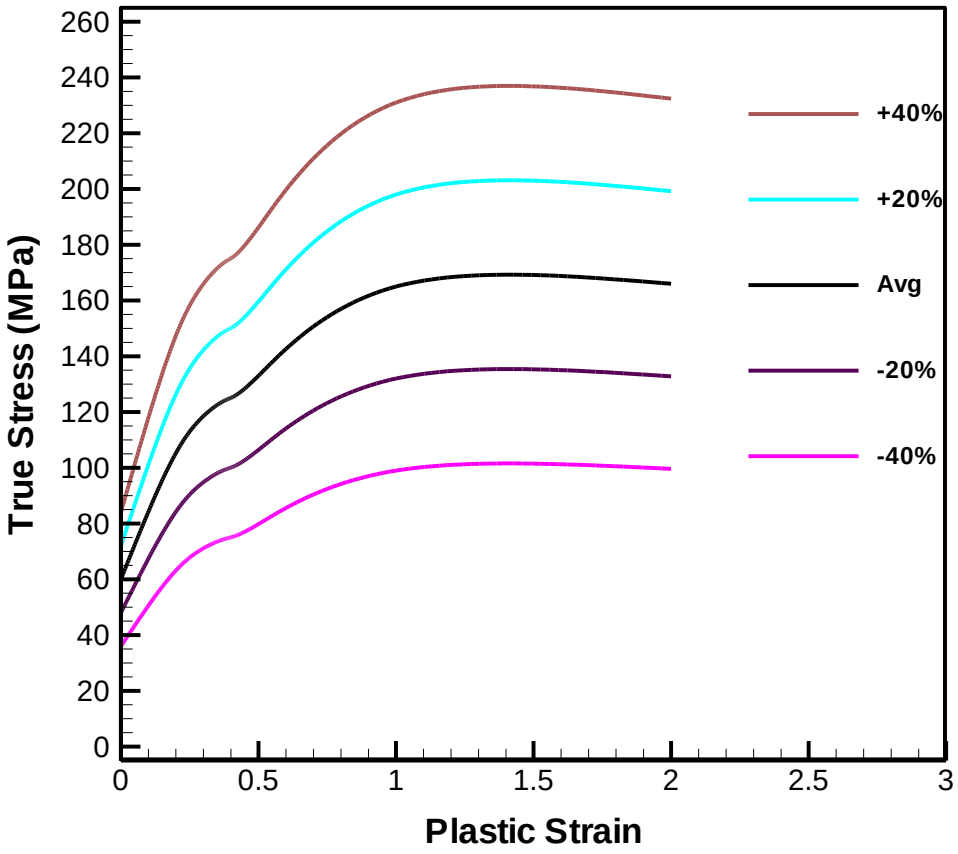

Figure 3.3: Plastic input properties

3.3 Modeling

The first step of the modeling is to obtain a computational geometry that contains grains. Voronoi tessellation was implemented to obtain the computational geometry where the grains were identifiable. At first a set of points was generated in MATLAB which were uniformly distributed. The corresponding Voronoi diagram consisted of a set of rectangles, each surrounding a point, as

shown in figure 3.4. The points were generated by: $x = \frac{D}{2} + (j-1) \times D$ and $y = \frac{D}{2} + (i-1) \times D$; where, D is the size of grains. For instance, $D = 420$ µm for the figure 3.5 and i, and j indicate number of row and column, respectively.

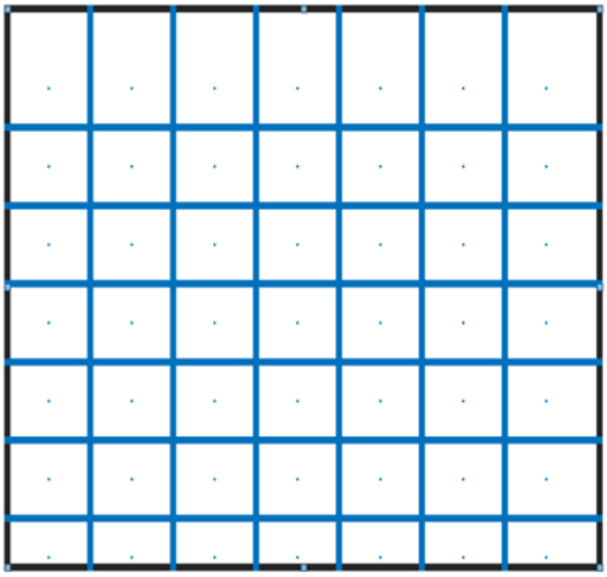

Figure 3.4: Rectangular Voronoi cells

In MATLAB, *voronoi(x, y)* syntax was used to generate a Voronoi diagram. In general, the grains are of irregular shapes. So, these points needed to be shifted randomly to several directions. To do that, a random number was incorporated to manipulate the coordinates of the points. The shifting coordinates *(x1, y1)* of the Voronoi cells were determined by: $x1 = x + r \times \frac{D}{2}$ and $y1 = y + r \times \frac{D}{2}$ .Where, (*x1, y1)* indicates updated coordinates of Voronoi cells and r is a randomly generated number between 0 and 1 in each iteration. A random number was generated by *r=abs((2*rand(1,1)-1))*.Then an updated Voronoi diagram (figure 3.5) was obtained by the command, *voronoi(x1,y1)*.

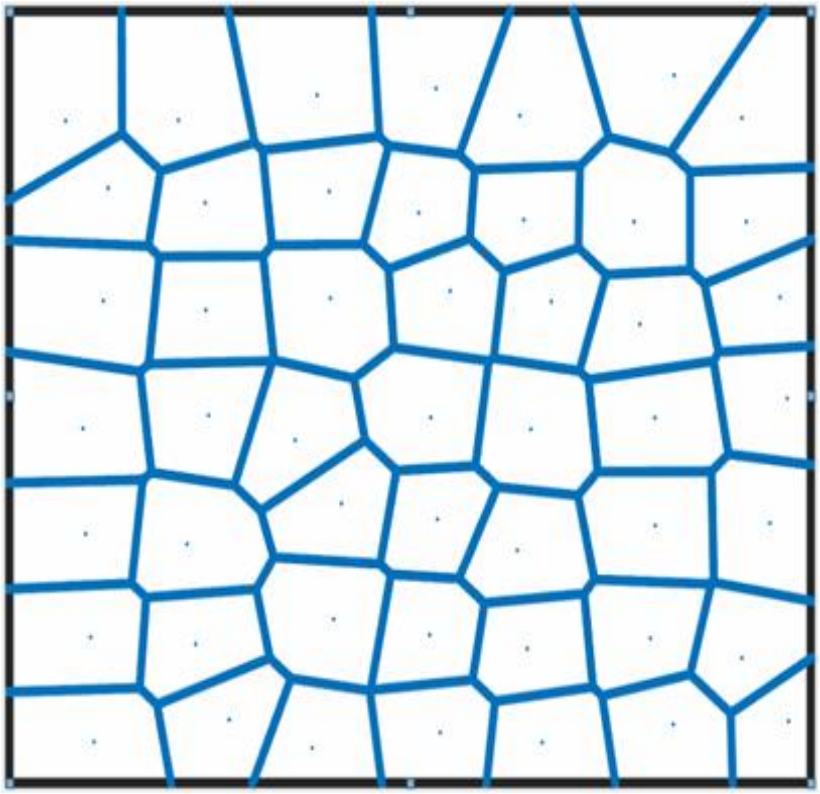

Figure 3.5: Irregular grain-like Voronoi cells

However, it was required to obtain a computational geometry with grains in ABAQUS for finite element analysis. In order to avail the vertices of each of the Voronoi cells and the sequences of their connectivity, a syntax, *[v,c] = voronoin([x1(:) y1(:)])* was used. Where, *v* indicates the set of points located at vertices of the Voronoi cells, and *c* indicates the sequence of connectivity to construct each of the Voronoi cells.

A python script was implemented into ABAQUS/CAE to obtain a 2-D planar wire frame (figure 3.6) from the vertices and the sequence of connectivity, obtained from MATLAB.

Figure 3.6: 2D wire-frame obtained in ABAQUS/ CAE

Afterwards, a geometry edit tool was used to convert each bounded wire frame to face with boundary (figure 3.7) so that each face could be assigned to material properties.

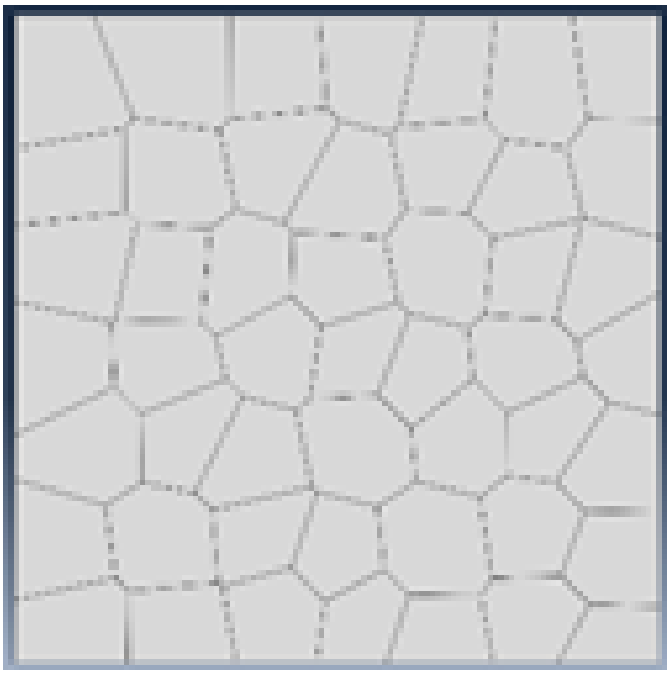

Figure 3.7: 2D surface texture for computation

With the help of python scripting, five sets of plastic properties from figure 3.3 were assigned to grains in a random fashion to get the computational geometry with heterogeneous material properties. Figure 3.8 shows the geometry with grains assigned to heterogeneous material properties.

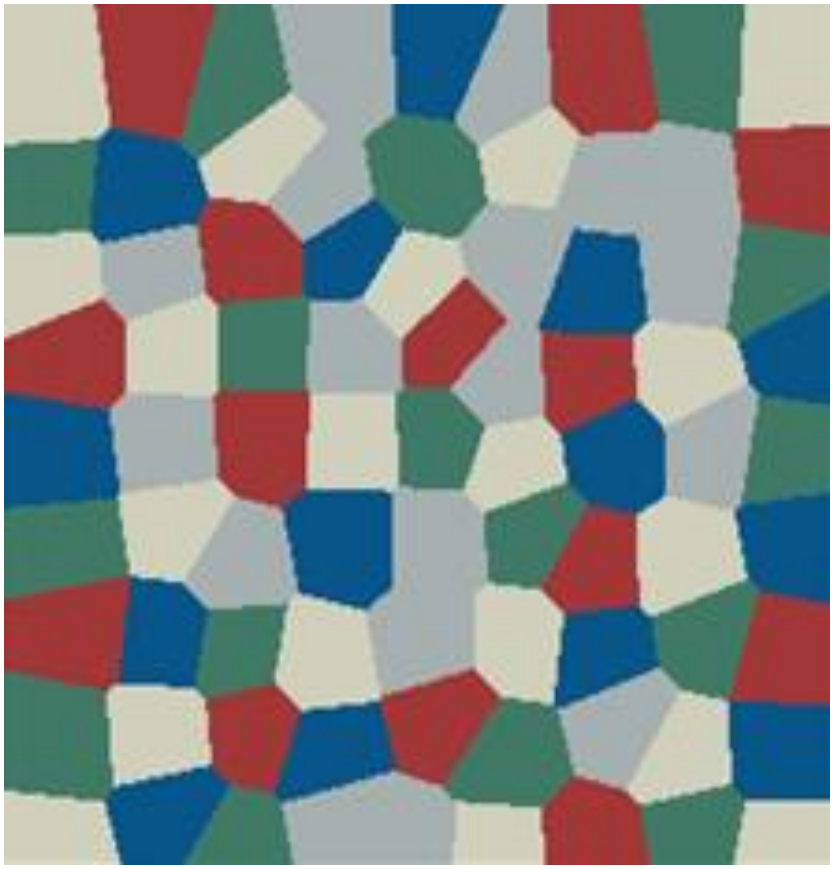

Figure 3.8: 2D computational domain with material heterogeneity

ABAQUS/Explicit was used to simulate the problem and predict the grain size effects. Dynamic/Explicit analysis was performed. The inside die-surface and outer billet-surface were in contact during extrusion. This contact was defined as penalty contact. A friction factor of 0.02 was used during computation. The geometry was then meshed prior to running simulations. The mesh structure is shown in the figure 3.9. The mesh type was free quad-dominated.

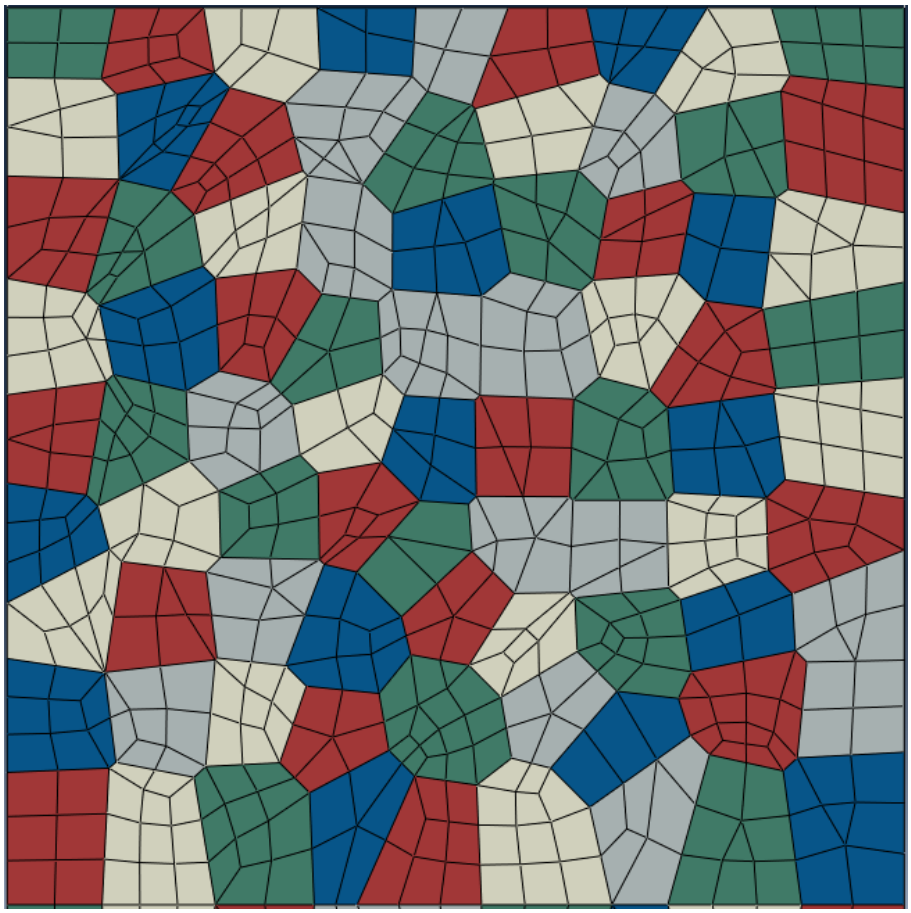

Figure 3.9: 2D computational domain with mesh

Boundary conditions:

The rigid die was imposed to stationary boundary conditions. The die was constrained in all directions. The billet motion was constrained in all directions except the vertical direction. The top-most surface of the billet was assigned to a velocity boundary conditions. The assigned speed was 1 mm/s downward.

3.4 Mesh Convergence

A mesh convergence test was performed for the model with 325 microns grain size. The simulation was run for five different numbers of elements. The von-Mises stress values were observed for a specific point, as shown in figure 3.10. The corresponding von-Mises values are

tabulated in table 3.1. From the figure 3.11, it is seen that the convergence occurs after the number of elements of approximately 4500.

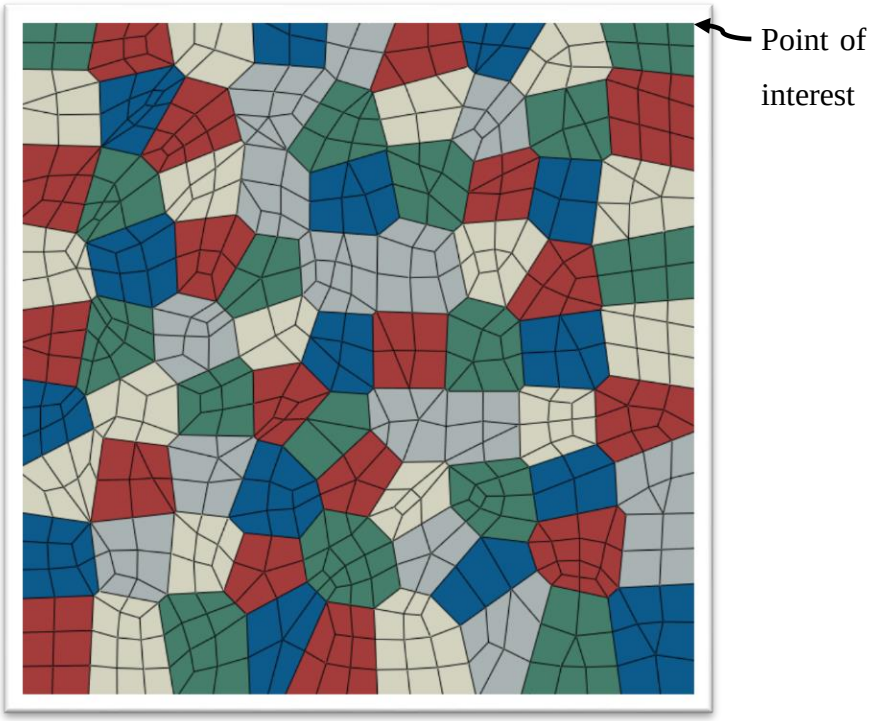

Figure 3.10: Mesh convergence test with the point of interest

Table 3.1: Von-Mises stress corresponding to number of elements for 2D forward extrusion model.

Number of elements	Von-Mises Stress (MPa)
1883	51.9483
2388	51.4183
3600	58.3847
4745	60.4621
5721	60.7184

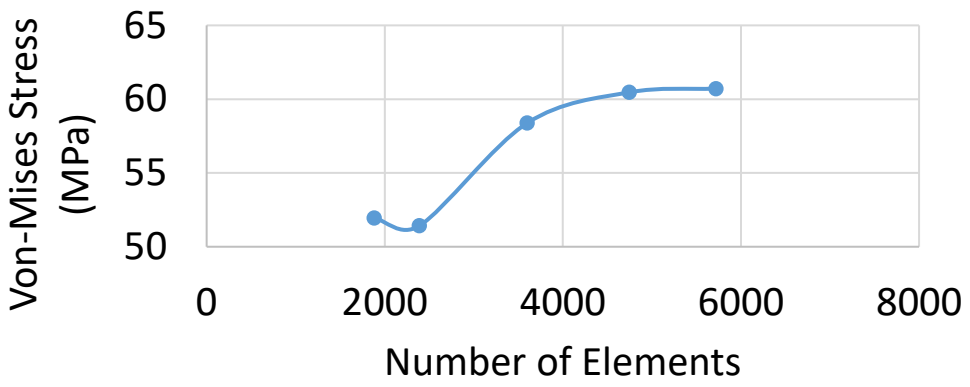

Figure 3.11: Plot of mesh convergence test for 2D forward extrusion

3.5 Simulation results

Equivalent plastic strain contours are shown in figure 3.12. Since the grains were assigned to non-homogeneous properties, all of the grains did not undergo uniform deformation. Therefore, non-uniform strain fields are observed for figures 3.12(b), 3.12 (c), 3.12 (d).

However, uniform strain fields are obtained for the model with homogeneous grain properties, as shown in figure 3.12 (a). It was expected that the periphery of the billet should experience large plastic strains; which is obvious in figure 3.12 (a). This trend is also seen in the figures 3.12 (a), (b), and (c), although the grains have heterogeneous material properties. Another noticeable response is observed in figure 3.12. The billet experiences bending after coming out from the die opening, except for the case of homogeneous grain properties. Therefore, a bending phenomenon is observed in small scale forward extrusion with non-homogeneous grain properties.

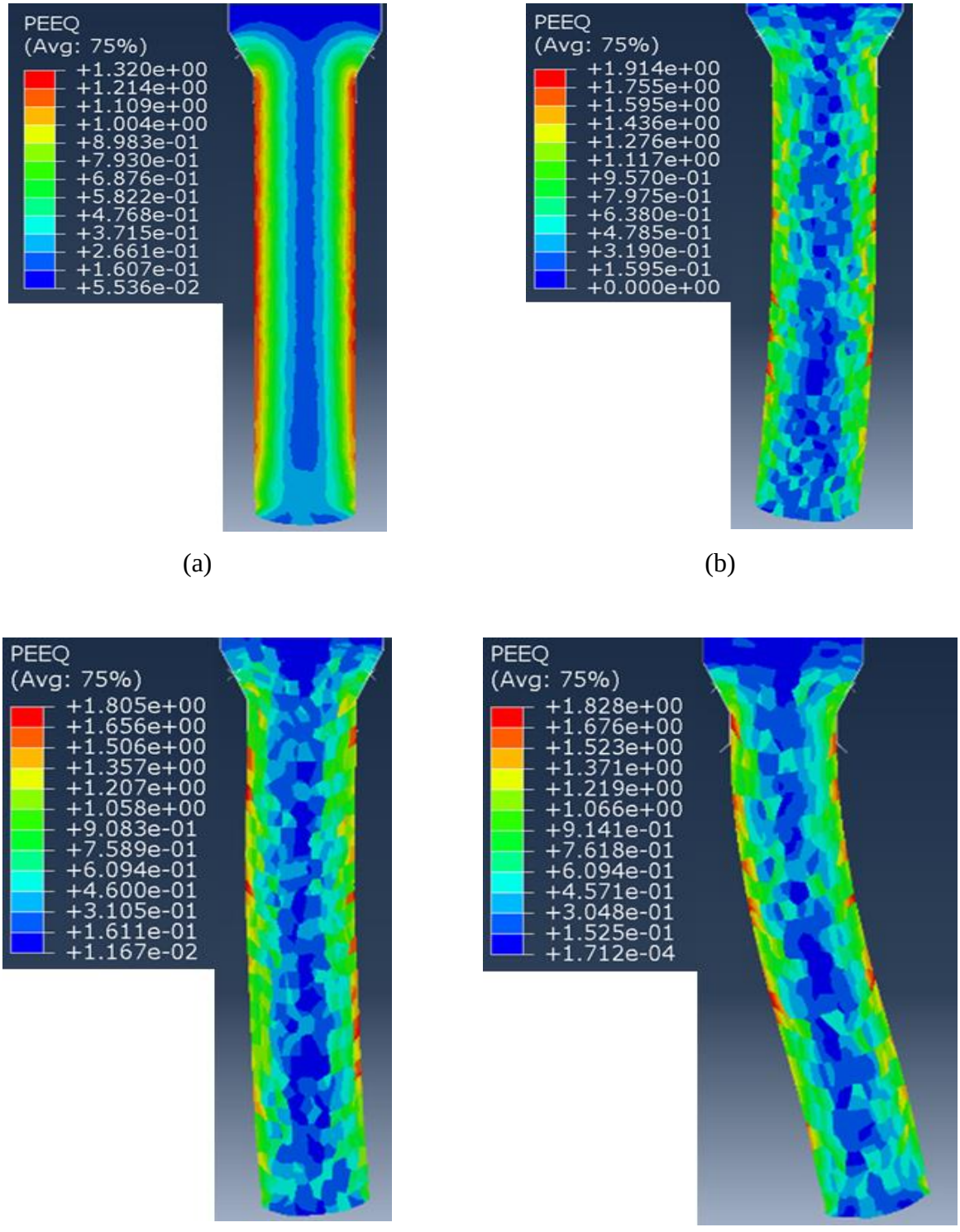

Figure 3.12: Equivalent plastic strain contours: (a) homogeneous (b) 291 µm, (c) 325 µm, and (d) 420 µm

Virtual grain morphologies before and after the extrusion are shown in figure 3.13. It is noticed that the grains at the surface experienced the maximum deformation. These grains came into direct contact with the die surface.

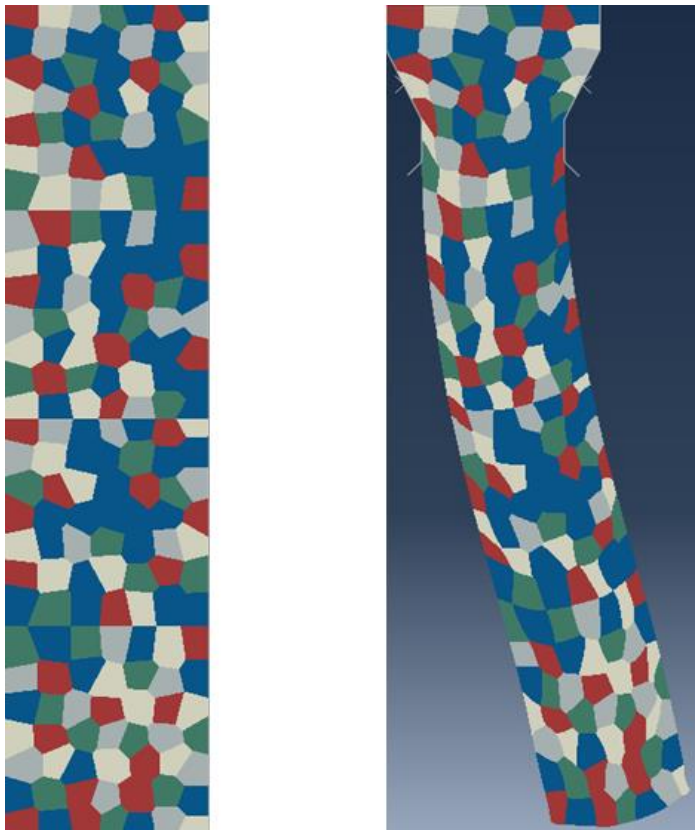

(a) (b)

Figure 3.13: Virtual grain morphology for 2D model: (a) before extrusion, (b) after extrusion

The magnitude of the lateral deflection of the billet tip was plotted against the downward movement. As the billet comes down the bottom surface of the billet deflects along the lateral direction. Figure 3.14 shows the relative magnitude of the lateral deflection for different grain sizes. It is obvious that magnitude of the lateral deflection increases with the increase in the size of grains. The maximum deflection was obtained for specimens with 420 micron grain size. No deflection was found for homogeneous specimen.

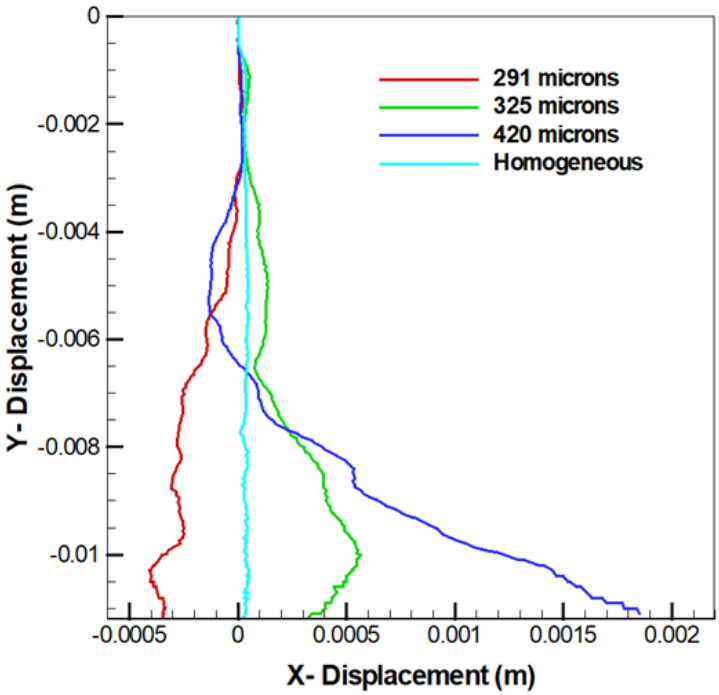

Figure 3.14: Lateral deflection of the 2D billet while extrusion

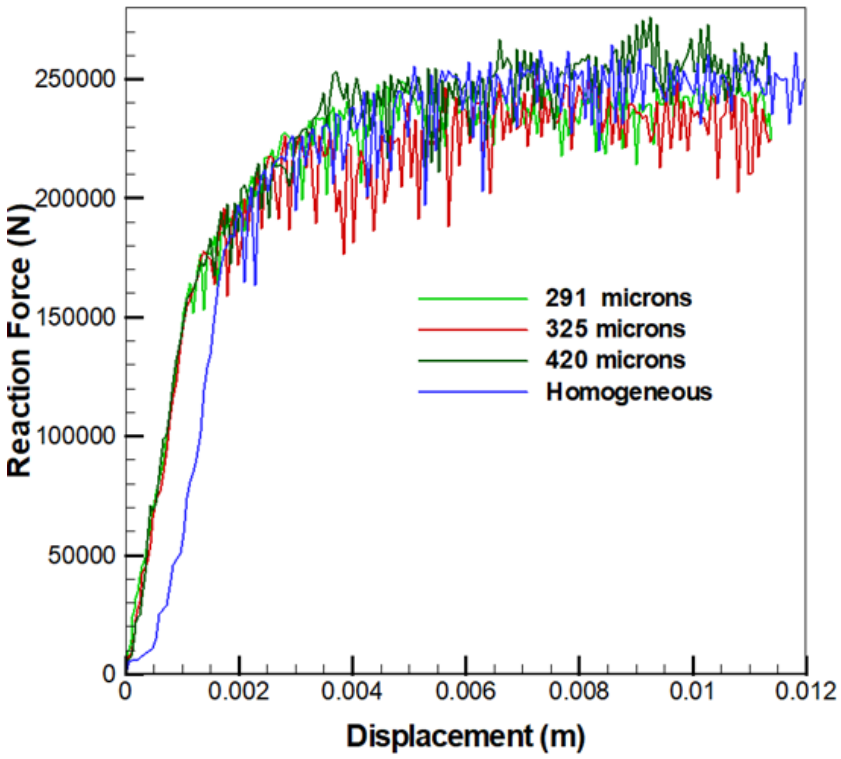

Figure 3.15: Load vs displacement plots for 2D model

Punch load requirements for different grain size specimens are shown in figure 3.15. The plots show a rapid increase of load at the beginning. Initially the punch squeezes the material before the onset of plastic deformation. The figure shows ups and downs in load requirements after the billet comes close to the die opening. Since the geometry consists of grains and all of the grains responded differently, load requirements varied very quickly with displacement.

Chapter 4

3D modeling of forward extrusion

2D modeling of forward extrusion was discussed in chapter 3. Although the 2D model does not represent actual physical scenario, it conveys important information of bending response and relative magnitude with grain size in small scale forward extrusion. In this chapter, a 3D model of forward extrusion will be discussed and grain size effects will be investigated on bending response of small scale forward extrusion.

4.1 Problem statement

Likewise the previous chapter, the billet material was aluminum. The die was considered as rigid body. The billet is in the shape of cylinder. The inner side dimension of the die cavity was equal to the outer diameter of billet. The die opening had the dimension of 2/3rd of the die cavity. The computation was performed for a billet diameter of 3 mm and a billet length of 3 mm. The die opening had a diameter of 2 mm and die angle of 23.57 degrees with the vertical.

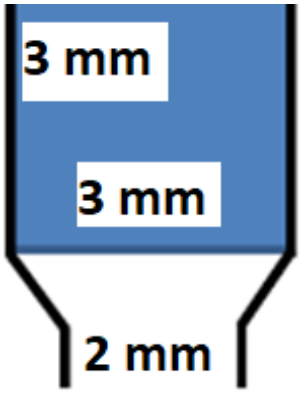

Figure 4.1: Schematic of the billet and die assembly for 3D model

4.2 Modeling

Half of the billet was considered for computation to reduce the computational cost. The cutting plane was imposed to appropriate symmetry boundary conditions. The one-half of the model had 200 grains in total.

Geometry and mesh:

Geometry and mesh were obtained using the software, Neper [49, 50, 51], which works on Linux architecture. The type of the mesh was C3D10, meaning 10 node nonlinear tetrahedral element. The billet geometry with mesh is shown is figure 4.2.

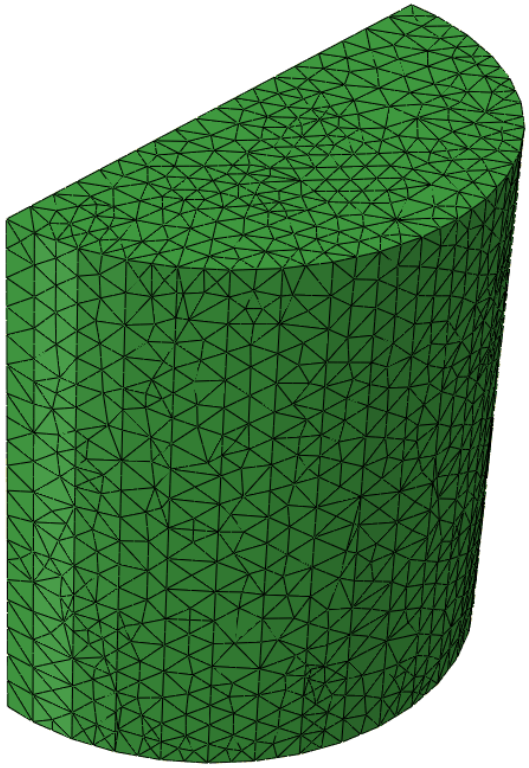

Figure 4.2: Geometry and mesh of the billet for 3D model

The die was considered as rigid material and the die-work piece assembly is shown in figure 4.3.

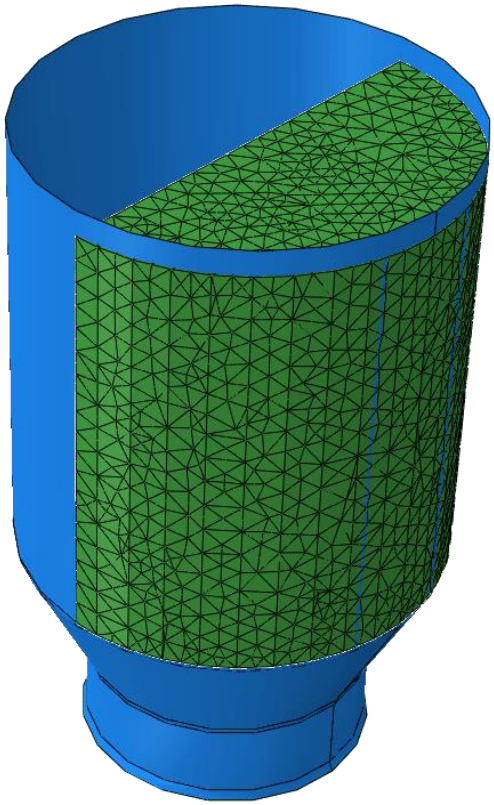

Figure 4.3: Die-billet assembly of 3D model

Assignment of properties:

A set of 5 different properties (set-1), as shown in figure 3.4 was assigned in random fashion among the grains to obtain grain heterogeneity. Also, a set of 11 different properties (set-2), as shown in figure 4.4 was used to assign grain heterogeneity.

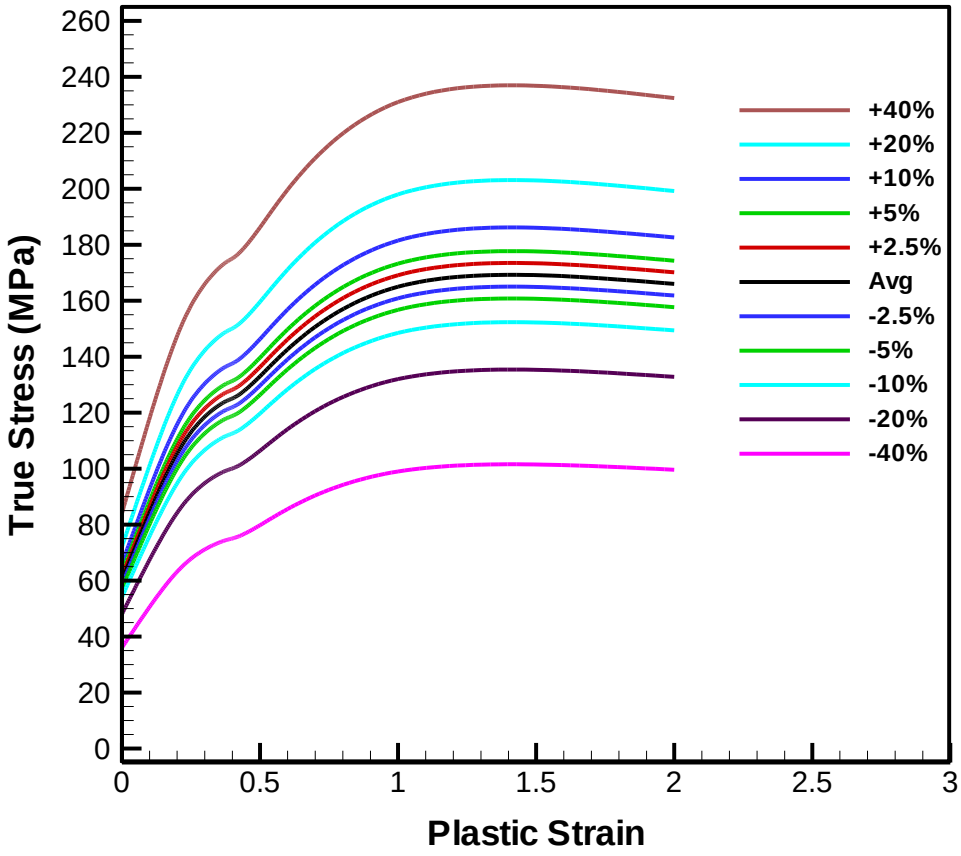

Figure 4.4: Plastic property inputs

A python script was run to assign plastic properties among the grains at a random fashion. After assigning the plastic input properties, the geometry became as shown in figure 4.5.

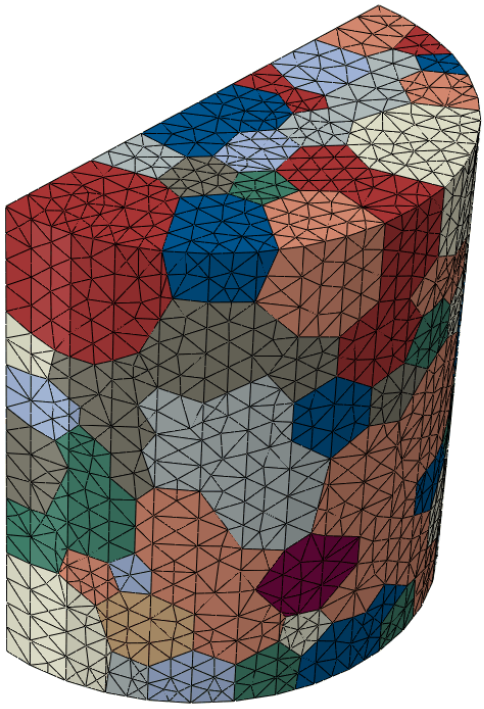

Figure 4.5: Geometry with assigned material heterogeneity

Interactions:

A friction contact was defined with penalty formulation to define the interaction between the billet surface and the inner die surface. A friction factor of 0.1 was used for the simulation. The contact type was hard, which means the contact surfaces will not allow penetration.

Boundary conditions:

The rigid die was considered fixed, i.e., zero degree of freedom. The top surface of the billet was restrained to the movement in vertical direction only. The cutting plane was imposed with a symmetry boundary condition so that its motion is constrained along the normal direction of the plane.

4.3 Mesh convergence

A mesh convergence test was performed for the model with 200 grains. The simulation was run for five different number of elements. The von-Mises stress values were observed for a specific point, as shown in figure 4.6. The corresponding von-Mises values are tabulated in table 4.1. From the figure 4.7, it is seen that the convergence occurs after the number of elements of approximately 30000.

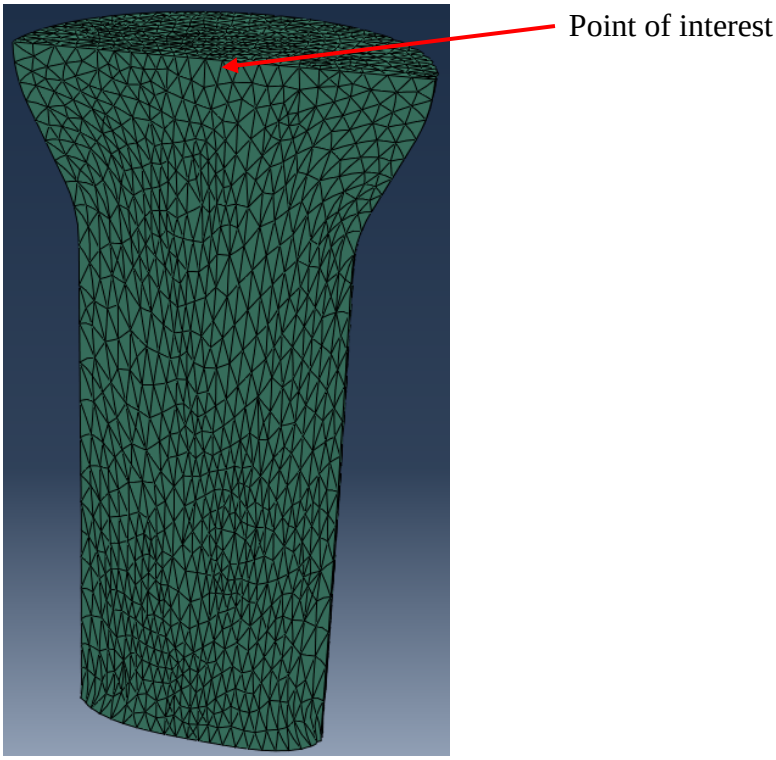

Figure 4.6: Mesh with point of interest for mesh convergence

Table 4.1: Von-Mises stress corresponding to the number of elements for 3D forward extrusion model.

Characteristic length (cl)	Number of elements	Von-Mises stress (MPa)
0.30	11974	114.56
0.22	16804	116.90
0.19	25964	118.68
0.15	43555	118.78
0.12	52932	118.60

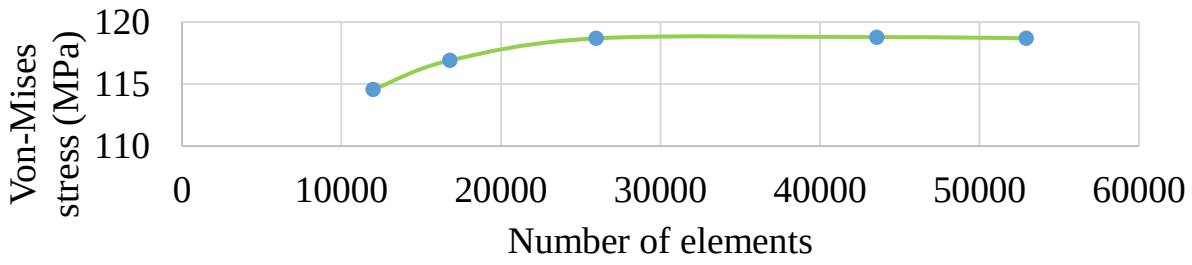

Figure 4.7: Mesh convergence test for 3D extrusion model simulation

4.4 Simulation results

Grain morphology was observed after the simulation. The grain morphology is shown in figure 4.8. The grains at the surface region undergo the maximum deformation. Also, the billet bends after the extrusion. But the bending phenomenon was not noticed for the specimen with homogeneous grain properties. So the reason of bending response can be explained by material heterogeneity, which was found for 2D model in chapter 3 as well.

A load vs displacement plot was obtained, as shown in figure 4.9. From the beginning of the process the load requirement increases rapidly up to a displacement of approximately 1 mm. Beyond that point, load decreases as the punch moves downward. The trend is as expected, because initially it requires load to cause elastic deformation until it reaches plastic region.

Figure 4.8: Grain morphology after extrusion: (a) front view (homogeneous), (b) rear view (homogeneous), (c) front view (set-1), (d) rear view (set-1), (e) front view (set-2), (f) rear view (set-2)

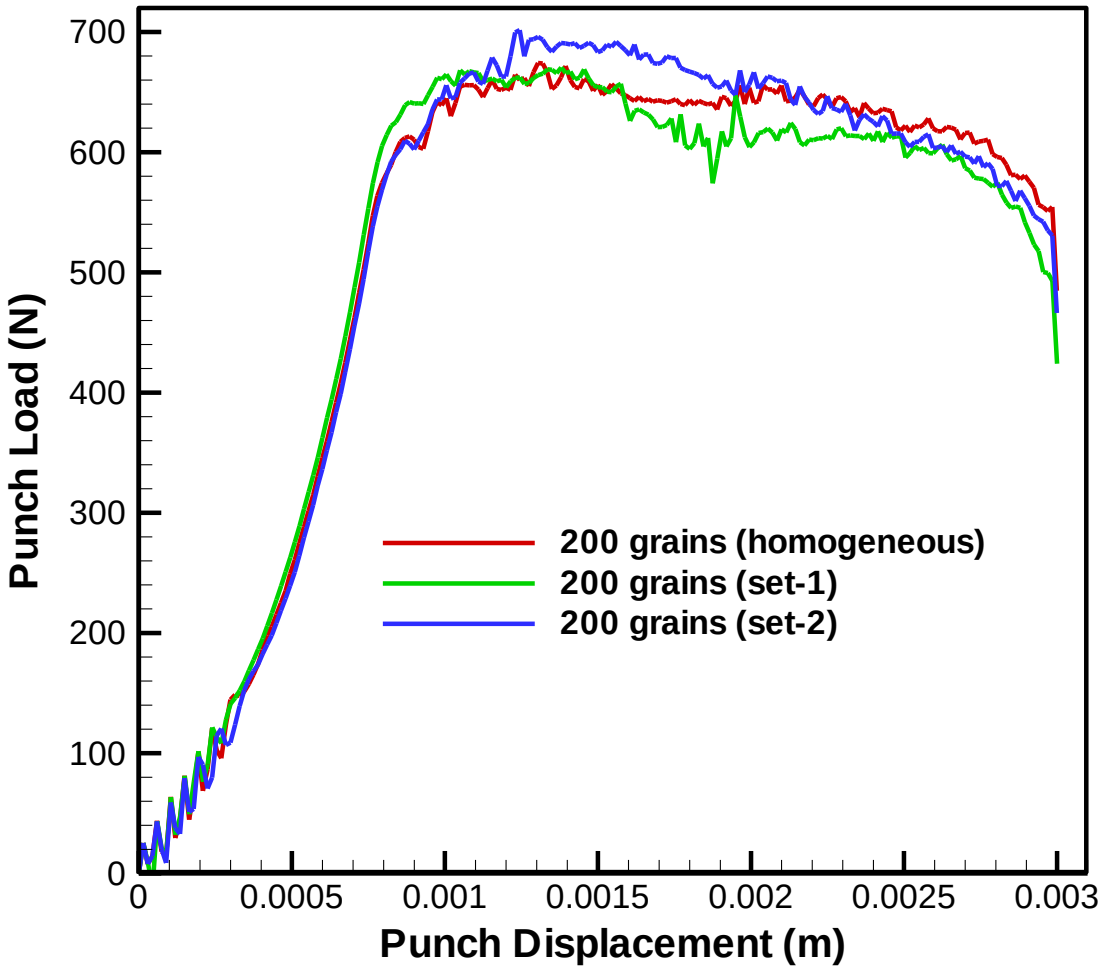

Figure 4.9: Load-displacement plots for 3D forward extrusion model

Lateral displacement vs vertical displacement was plotted, as shown in figure 4.10. The plots show that the billet tip moves laterally as it moves down. The set-1 had a greater material scatter, relative to set-1. The bending magnitude was greater for set-1.

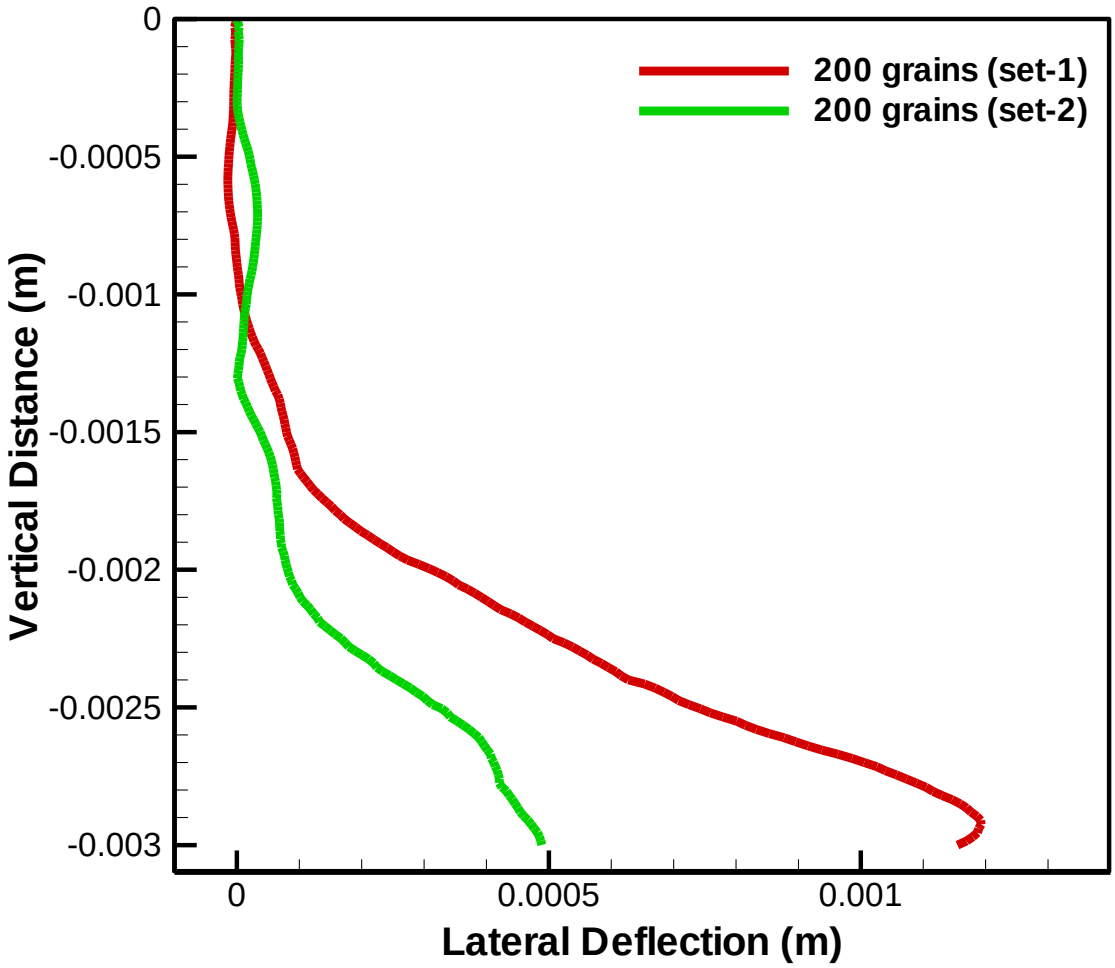

Figure 4.10: Lateral displacement plots with vertical movement for 3D model

4.5 Comparative case study

A comparative case study was performed using experimental results obtained by Krishnan et al. [52]. Experiments were performed for microscale forward extrusion. The experimental details are given in Krishnan et al. [52]. The die of the experiment is shown in figure 4.11. The average grain size was 211 microns. A model was developed to mimic the experimental set up with same die dimensions and with average grain size of 211 microns. Figure 4.12 shows the die that was drawn to model the forward extrusion. The billet shape was cylindrical and half of the billet was considered for computational purposes. The diameter and length of the billet were 0.76 mm and 3 mm, respectively. A polycrystal geometry was obtained with a grain size of 211 microns.

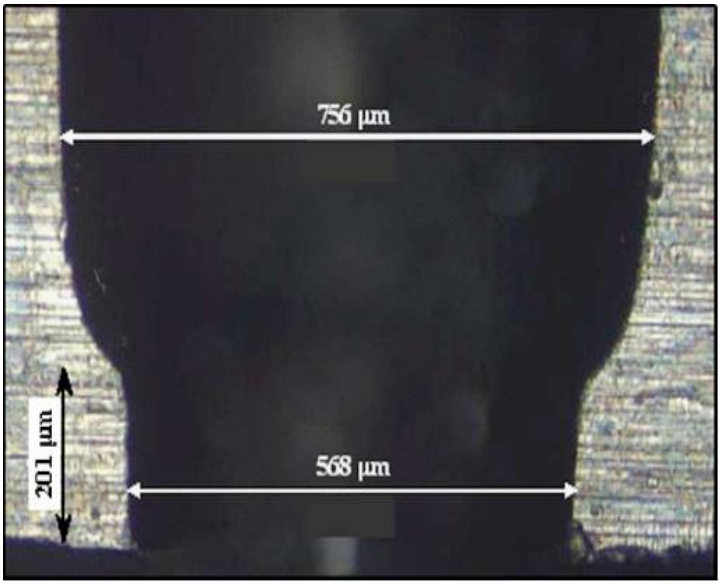

Figure 4.11: Die configuration for the experiment [52]

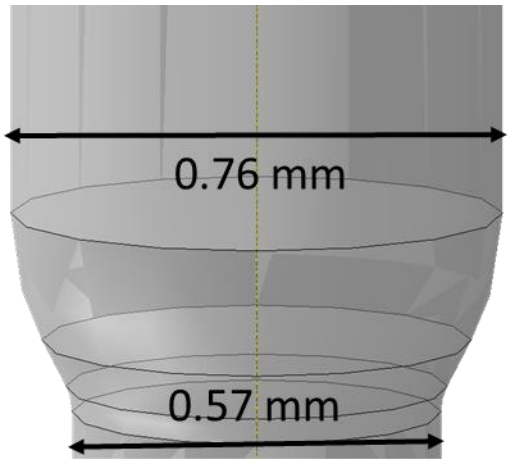

Figure 4.12: Die drawn for modeling

The bending response was found from the simulation. Then the bending deflection magnitude was quantified and compared with the extracted deflection magnitudes from literature [52], as shown in figure 4.13. Set-1 indicates higher degree of material non-homogeneity, and set-2 indicates lower degree of material non-homogeneity. If maximum magnitude of the deflection is considered, property set-1 predicts closer than the set-2.

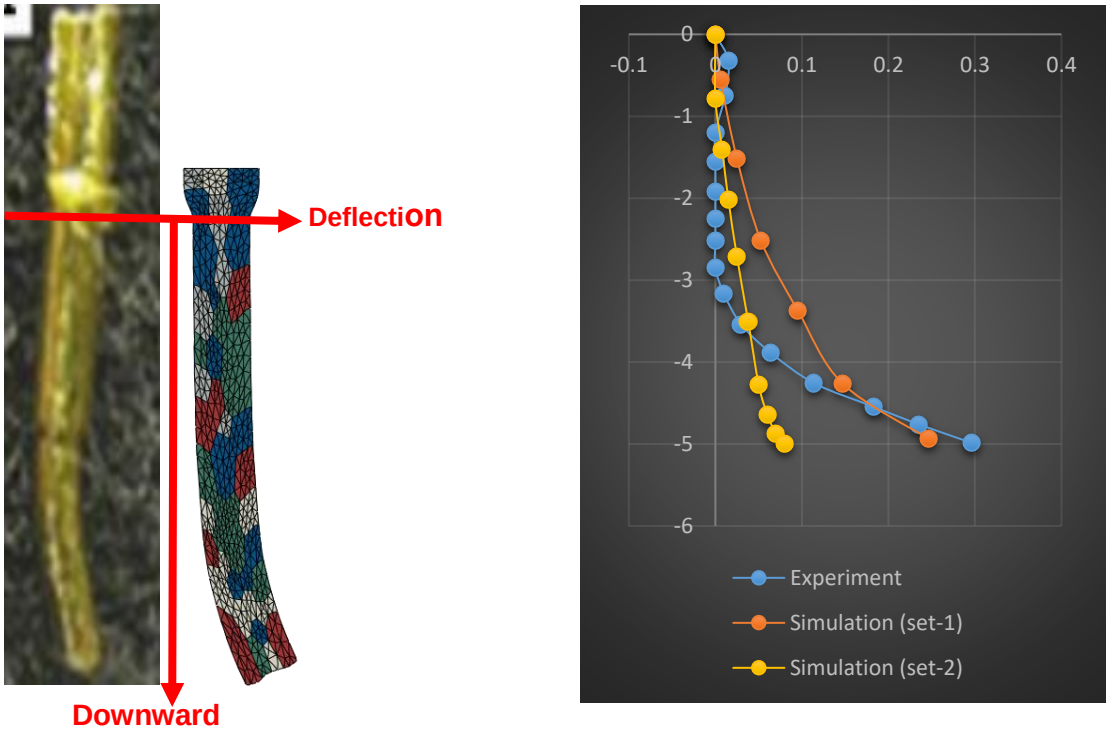

Figure 4.13: Bending deflection comparison (all units are in mm)

The simulation was done for different grain sizes with the same die configuration. It was found that the deflection magnitude increases as the grain size increases, as shown in figure 4.14.

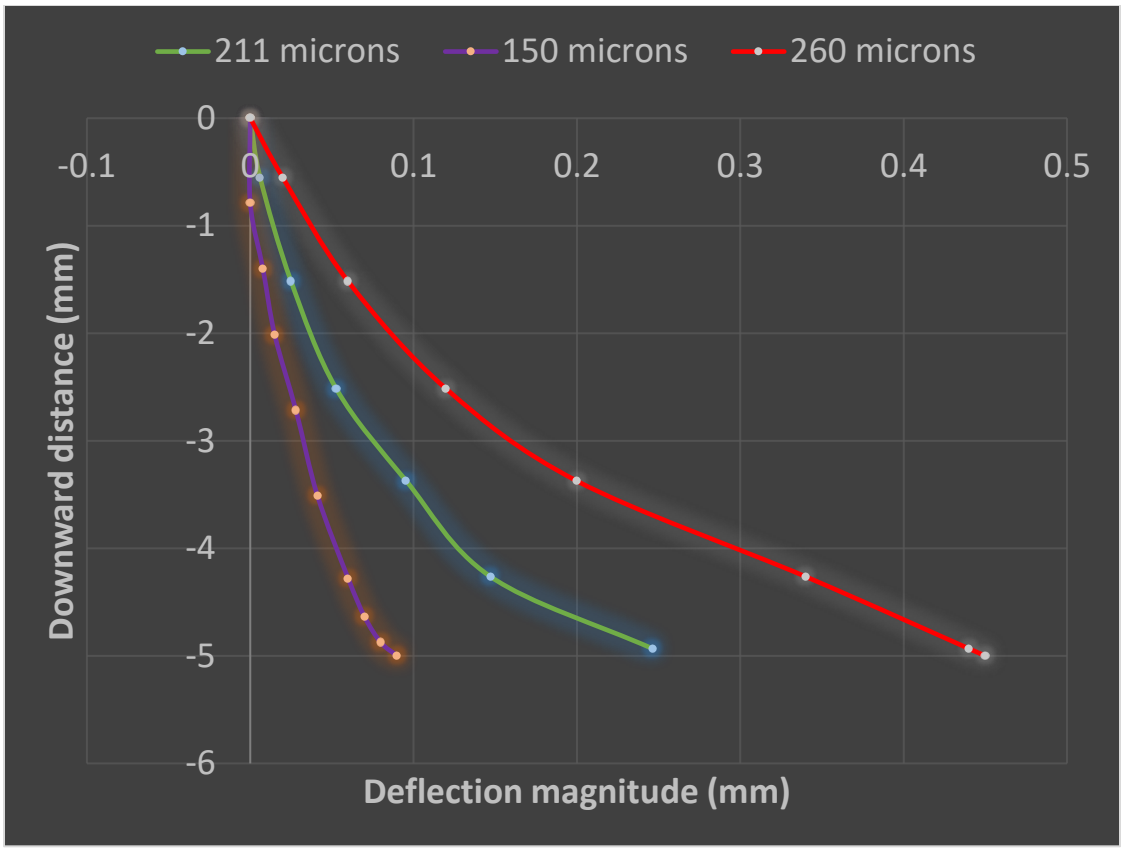

Figure 4.14: Comparison of the deflection magnitude for different grain size specimens

4.6 Full modeling of 3D forward extrusion

Previous sections of this chapter were concerned with the half model of forward extrusion. Since grain heterogeneity is present, symmetry boundary conditions cannot mimic the actual case perfectly. However, a half model is a good approximation to predict the bending phenomenon with lower computational cost. The full billet with material heterogeneity is shown in figure 4.15.

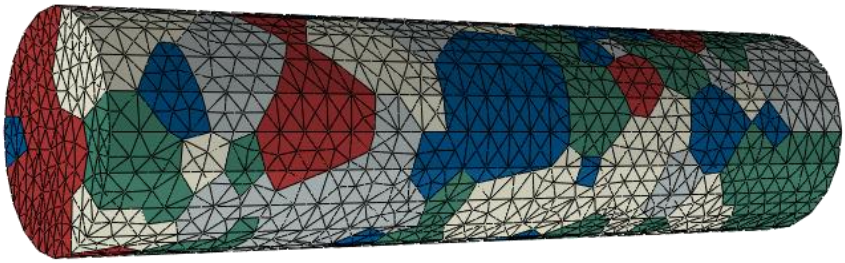

Figure 4.15: 3D billet with material non-homogeneity

The billet geometry contains 192 grains with an average grain size of 211 microns. Like the half model, the die was rigid body and the fixed boundary conditions were applied. Figure 4.16 shows the final shape of the billet after extrusion.

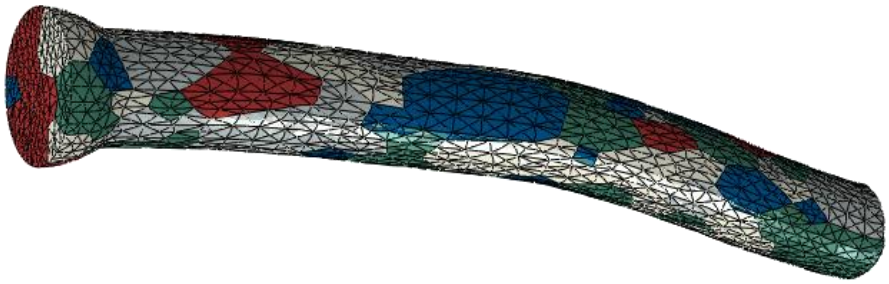

Figure 4.16: Final shape of the extruded part

The comparison between the simulation and the experimental [11] outcomes are compared in the figure 4.17.

Figure 4.17: Comparison between experimental and computational deflection magnitudes (all units are in mm)

Chapter 5

Hemispherical Bowl-shaped forming with cover plate

5.1 Problem statement

Circular billets of diameter 15 mm were used as the work piece. The thickness varied from 0.4 mm to 0.8 mm, and the hemispherical die and punch had a diameter of 10 mm. It was confirmed from initial experiments that without a cover a plate, crinkles are observed; these were more obvious in thinner specimens. Therefore, a cover plate was introduced to prevent the formation of crinkles, and hence to achieve smooth final forms. The cover plate successfully restrained the billet movement in the vertical direction. The downward displacement of the punch was 5 mm, which is the radius of the punch and die cavity. The relative position of die, punch, work piece, and cover plate is shown in figure 5.1, as an assembly.

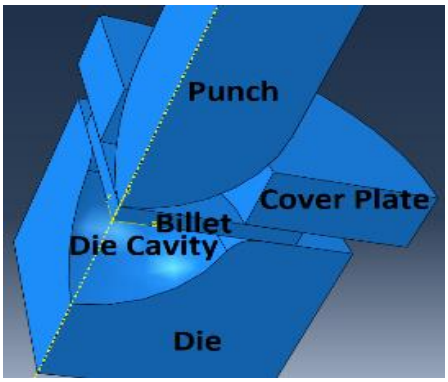

Figure 5.1: Assembly

5.2 Modeling

One-quarter of the comprehensive set up, as shown in figure 5.1 was considered to reduce the computational cost, applying appropriate symmetry boundary conditions at the cutting planes. The commercial FE software Abaqus/Standard was used to simulate the problem stated in section

5.1. The input material properties of the die, punch, and the cover plate were obtained from the experimental stress-strain plot in figure 5.2, and plastic input properties of the billet material were obtained from the true stress vs plastic strain plot in figure 5.3.

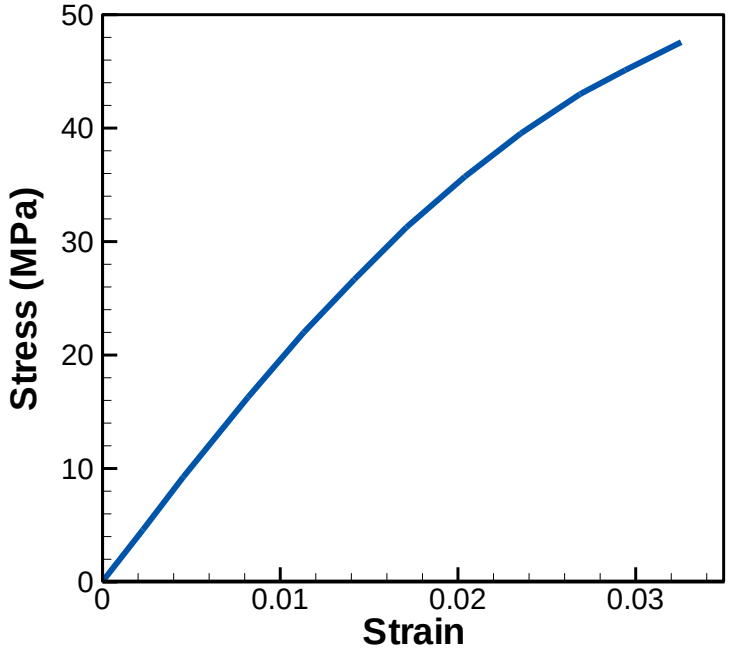

Figure 5.2: Stress-strain plot for SLA resin

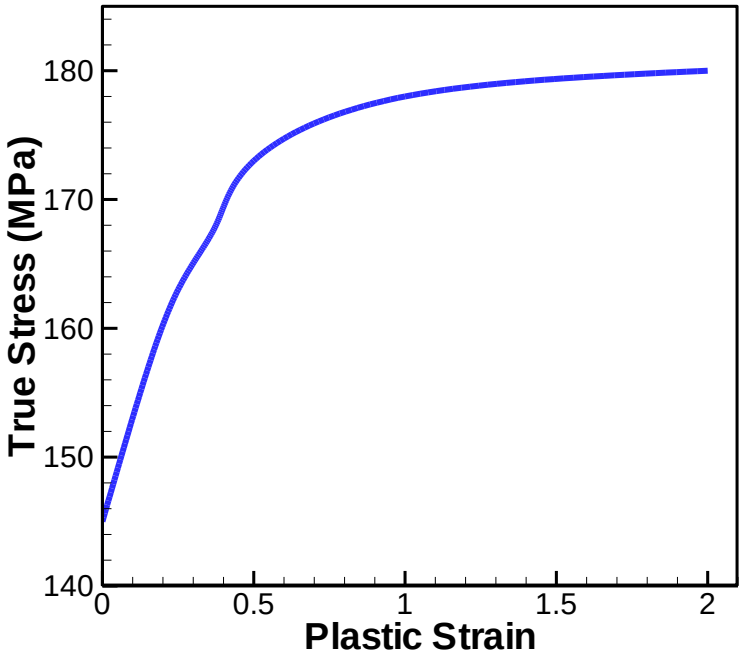

Figure 5.3: Stress-strain plot for 3003-H14 Al alloy

The contact surfaces were defined as frictional contact, and a penalty formulation was used with a friction factor of 0.1. A structured hexagonal mesh was used for billet and cover plate, and free tetrahedral mesh was used for the punch and die. Symmetry boundary conditions were imposed at the cutting planes of all entities. Fixed boundary conditions were imposed at the bottom of the die. A displacement boundary condition of 5 mm downward was imposed on the punch.

5.3 Mesh convergence test

A mesh convergence test was performed for the model with 0.4 mm thickness. The simulation was run for six different numbers of elements. The von-Mises stress values were observed for a specific point, as shown in figure 5.4. The corresponding von-Mises values are tabulated in table 5.1. From the figure 5.5, it is seen that the convergence occurs after the number of elements of approximately 250.

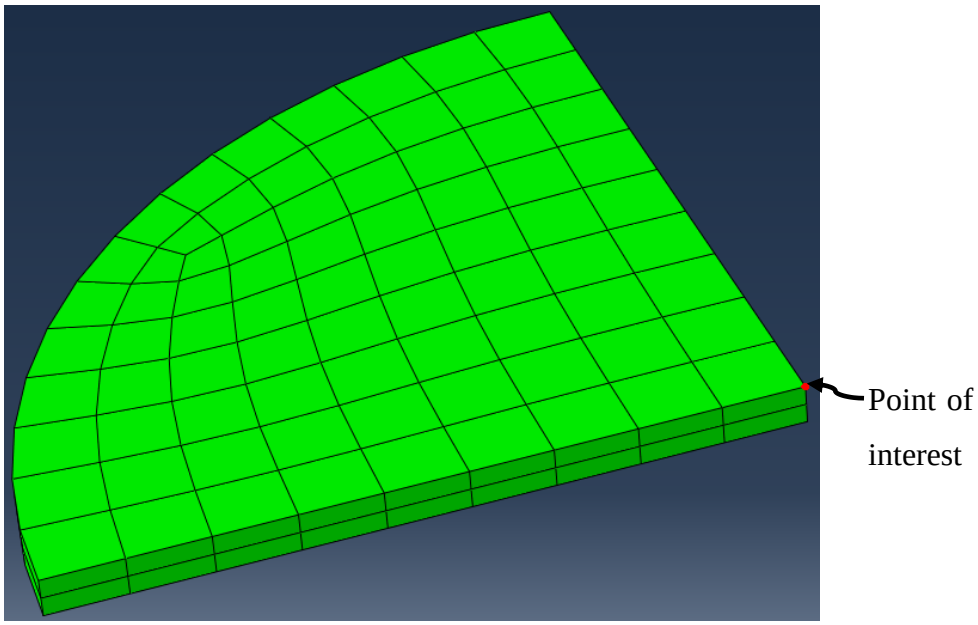

Figure 5.4: Mesh convergence of the sheet metal forming operation with point of interest

Table 5.1: Von-Mises stress corresponding to number of elements for metal forming simulation.

Number of elements	Von-Mises Stress (MPa)
120	154.147
154	155.304
212	159.04
320	158.879
652	158.906
1150	158.859

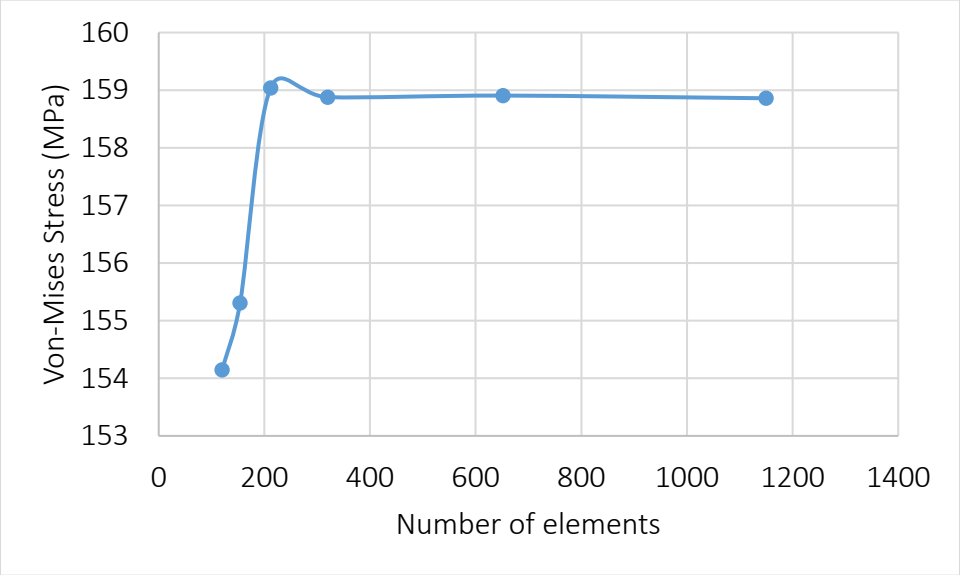

Figure 5.5: Mesh convergence test for metal forming simulation

5.4 Results

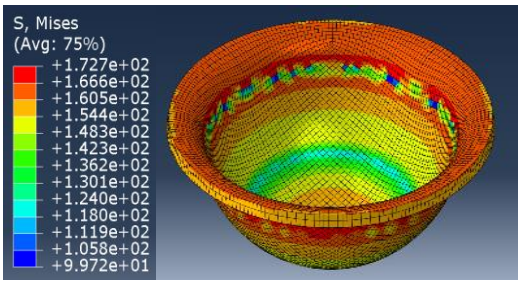

(a) 0.4 mm

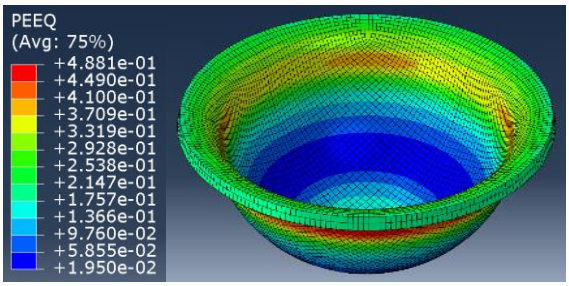

(a) 0.4 mm

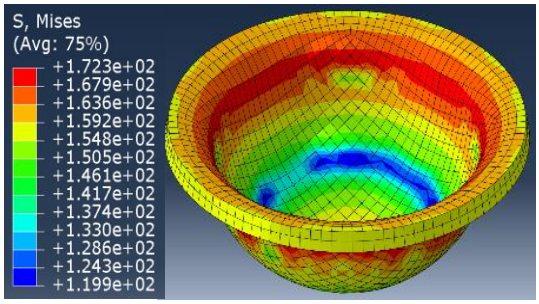

(b) 0.6 mm

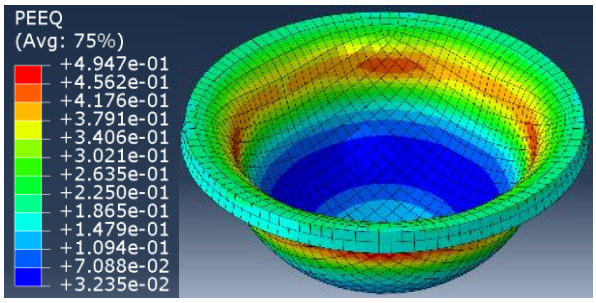

(b) 0.6 mm

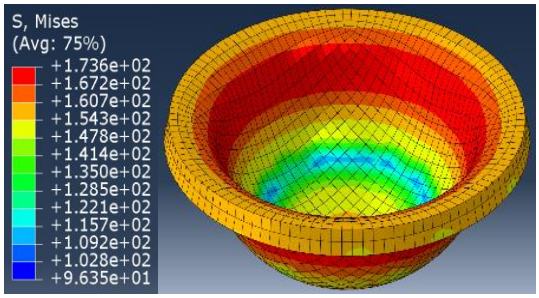

(c) 0.8 mm

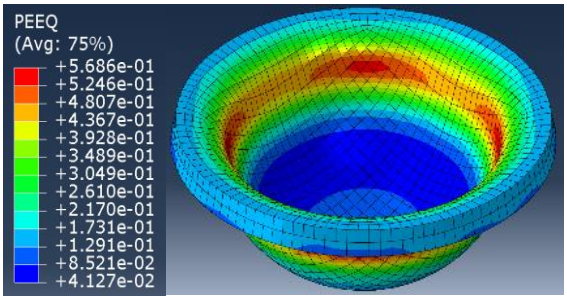

(c) 0.8 mm

Figure 5.6: von-Mises contours

Figure 5.7: Equivalent plastic strain contours

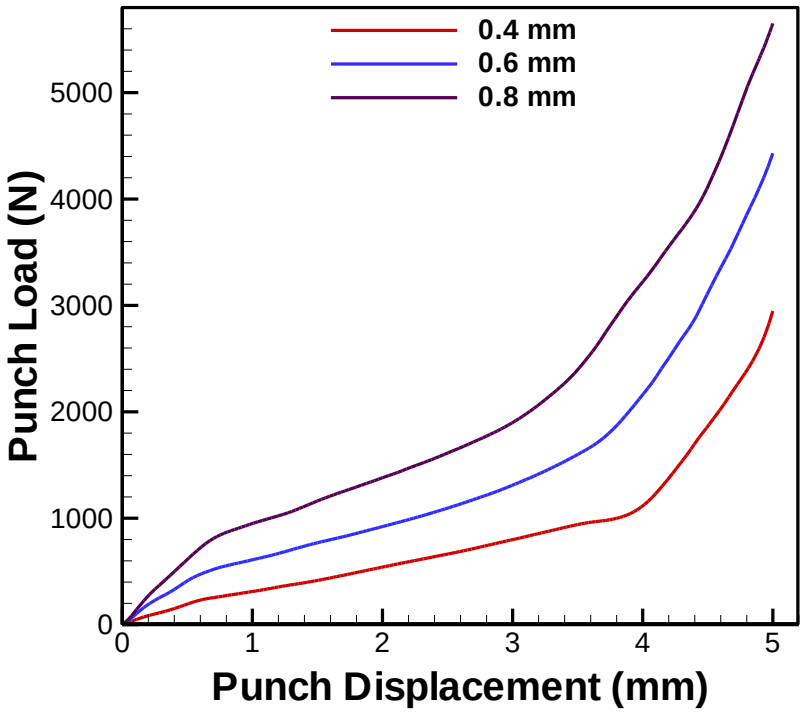

Figure 5.8: Load vs displacement plots

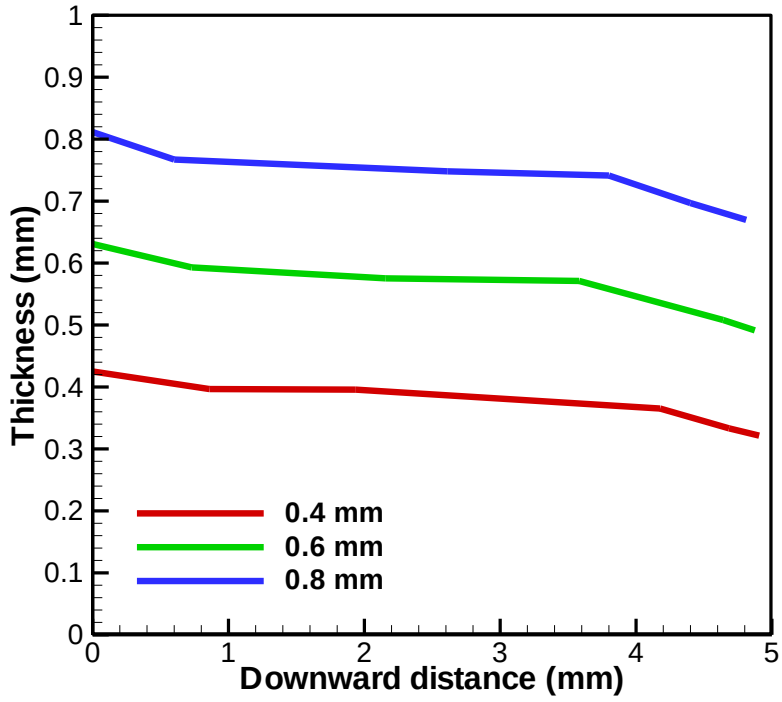

Figure 5.9: Thickness distribution of the final forms

Final form shapes for thicknesses of 0.4, 0.6, and 0.8 mm were obtained by simulation. The von-Mises stress contours (figure 5.6) and equivalent plastic strain contours (figure 5.7) were obtained and compared for different thicknesses. As the thickness of the billet increases, the maximum magnitude of the equivalent plastic strain increases. However, the maximum magnitude of the von-Mises stress remains similar at high strains. Punch load vs punch displacement plots (figure 5.8) were calculated and compared for different thickness specimens. Load requirement increases as the thickness increases, as expected. Finally, the thickness distribution was calculated and plotted for final form shapes (figure 5.9). Thickness increases gradually towards the periphery of the bowl.

There is a sharp transition in the load vs displacement plot for a 0.4 mm thick specimen at a displacement of approximately 4 mm, as shown in figure 5.8. However, for thicker specimens, this transition is not as obvious. The reason behind this phenomenon is the effect of bending response during deformation of the circular plates. Bending response is dominated in thicker specimens, whereas, membrane/tensile response is dominated in thinner specimens. Another aspect is noted in the figure 5.8 up to a punch displacement of approximately 0.8 mm; as the thickness of the specimen increases, the slope of the load-displacement plots increases significantly. This is because of the greater elastic force requirement to deform the thicker specimens before the onset of plastic deformation.

Thickness of the final form decreases gradually from periphery to the center of the bowl. This trend can be validated by the theoretical formulation [53] of thickness distribution.

5.5 Validation

Numerical predictions were validated by experimental results. Figure 5.10 shows the comparison of experimental and numerical load-displacement plots. The plots are in good agreement. At the start, simulation overestimates a little higher than the experimental load requirement. And towards the end, simulation underestimates a little lower than the experimental load requirement. Moreover, a little deviation is observed at the transition point of approximately 4 mm displacement. The reason of this little deviation could be the input material properties. The specimen was 0.4 mm thick, which was in sub-millimeter range. But the input properties were for

bulk material, obtained from tensile tests. So the response of small specimens could slightly deviate from the expectation.

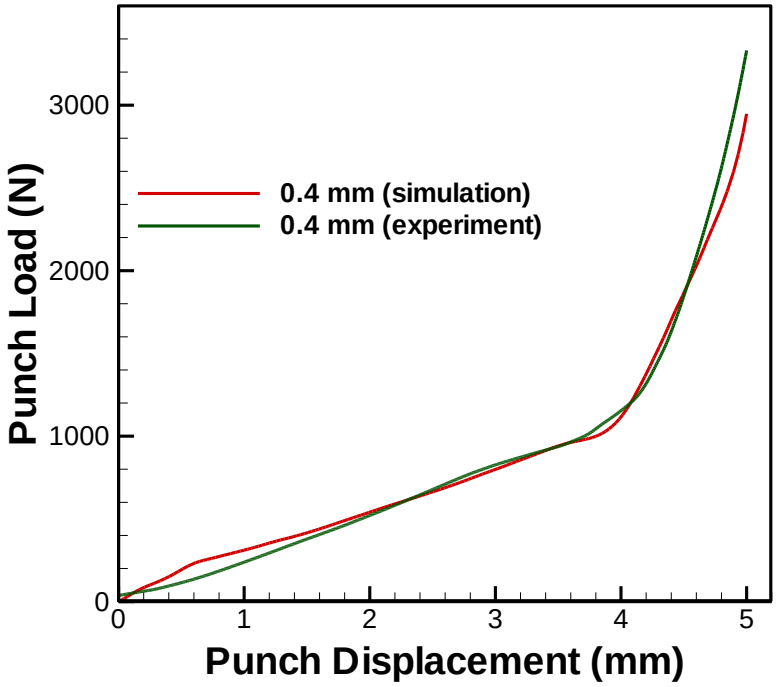

Figure 5.10: Validation of numerical metal forming simulation model

Chapter 6

Conclusions and Recommendations

6.1 Conclusions

Size effects have been studied. When the specimens are miniaturized, size effects play a significant role. As described in chapter 1, researchers found the influence of size effects in tensile tests. Flow stress increases as the thickness of the specimen increases. But the flow stress decreases as the grain size of the specimen increases. Due these influence of size effects, some unexpected problems arise in metal processing. One of the major problems is unexpected distortion of the final product. Theoretically researchers formulated methods to calculate flow stress during in simple tension or compression tests as mentioned in chapter 2. But for metal processing, high plastic deformation occurs and due to nonlinearity, theoretical formulation fails to predict the influence of size effects on process parameters. Therefore, numerical modeling was performed to predict size effects on metal processing.

In this study, the influence of grain size effects were investigated on small scale forward extrusion, and geometric size effects were studied on metal forming with a punch and die combination. It was shown in chapter 3 and 4 that due to material heterogeneity, size effects are observed. As the grain size increases, the magnitude of the bending response in small scale forward extrusion increases. Since the different grains had different material properties, all of the grains did not undergo the same strain. Due to property differences, the strain field differed significantly. The resultant effect of this non-uniform deformation contributes to a distortion phenomenon. For forward extrusion, this distortion phenomenon was observed as bending.

Geometric effects were investigated in chapter 5, in the case of a hemispherical forming process. Numerical simulations were performed and experiments were conducted. The simulation and the experimental results were in good agreement. The punch load requirements were greater for thicker specimens, as expected. It was observed that there were two distinctive regions in the load vs displacement plots. These are due to the different material response at different phases of the process. Initially the response was governed by a bending response, whereas, as the process

progresses beyond 80% of total displacements, the response is dominated by membrane/tensile response, especially for thinner specimens. Tensile response was more significant for thinner specimens, therefore, the sharp load-displacement transition was noticed.

6.2 Recommendations

Qualitative prediction of bending response was performed in this study. Therefore, experiments can be performed to validate the numerical model. Experiments for a number of different die-punch combinations can be conducted for a comprehensive investigation of size effects in small scale forward extrusion. Analyzing the experimental results can contribute to find a robust numerical model for predictions of size effects. Heat treatment can be performed to customize the grain size of the specimens and incorporating the heat treatment parameters into final predictions.

Forming can be performed for different shapes, such as cylindrical, cubic, tapered rectangular, etc. The obtained results can be compared for different shapes to correlate between different shapes. Grain size effects can be investigated for bowl-shaped forming.

References

1. Vollertsen, F. (2008). Categories of size effects. *Production Engineering*, *2*(4), 377.
2. Liu, J. G., Fu, M. W., Lu, J., & Chan, W. L. (2011). Influence of size effect on the springback of sheet metal foils in micro-bending. *Computational Materials Science*, *50*(9), 2604-2614.
3. Jiang, Z., Zhao, J., & Xie, H. (2017). *Microforming technology: theory, simulation and practice*. Academic Press.
4. Ma, X., Lapovok, R., Gu, C., Molotnikov, A., Estrin, Y., Pereloma, E.V., Davies, C.H.J. and Hodgson, P.D., 2009. Deep drawing behaviour of ultrafine grained copper: modelling and experiment. *Journal of materials science*, *44*(14), pp.3807-3812.
5. Kals, T. A., & Eckstein, R. (2000). Miniaturization in sheet metal working. *Journal of Materials Processing Technology*, *103*(1), 95-101.
6. Li, H.Z., Dong, X.H., Shen, Y., Zhou, R., Diehl, A., Hagenah, H., Engel, U., Merklein, M. and Cao, J., 2012. Analysis of microbending of CuZn37 brass foils based on strain gradient hardening models. *Journal of Materials Processing Technology*, *212*(3), pp.653-661.
7. Engel, U. (1998). Cold forging of *microparts* . *Proc. 1st ESAFORM* , 77-80.
8. Vollertsen, F., & Hu, Z. (2006). Tribological size effects in sheet metal forming measured by a strip drawing test. *CIRP annals*, *55*(1), 291-294.
9. Chan, W. L., Fu, M. W., Lu, J., & Liu, J. G. (2010). Modeling of grain size effect on micro deformation behavior in micro-forming of pure copper. *Materials Science and Engineering: A*, *527*(24-25), 6638-6648.
10. Stachowicz, F., Trzepieciński, T., & Pieja, T. (2010). Warm forming of stainless steel sheet. *Archives of Civil and Mechanical Engineering*, *10*(4), 85-94.

11. Parasiz, S. A., Kinsey, B., Krishnan, N., Cao, J., & Li, M. (2007). Investigation of deformation size effects during microextrusion. *Journal of Manufacturing Science and Engineering*, *129*(4), 690-697.

12. Meyersm, M. A., & Ashworth, E. (1982). A model for the effect of grain size on the yield stress of metals. *Philosophical Magazine A*, *46*(5), 737-759.

13. Fu, H. H., Benson, D. J., & Meyers, M. A. (2001). Analytical and computational description of effect of grain size on yield stress of metals. *Acta materialia*, *49*(13), 2567-2582.

14. Cailletaud, G., Diard, O., Feyel, F., & Forest, S. (2003). Computational crystal plastiticy: from single crystal to homogenized polycrystals. *Technische Mechanik*, *23*, 130-145.

15. Aurenhammer, F. (1991). Voronoi diagrams—a survey of a fundamental geometric data structure. *ACM Computing Surveys (CSUR)*, *23*(3), 345-405.

16. Okabe, A., Boots, B., Sugihara, K., & Chiu, S. N. (2009). *Spatial tessellations: concepts and applications of Voronoi diagrams* (Vol. 501). John Wiley & Sons.

17. Li, Q., & Lovell, M. (2008). Cross wedge rolling failure mechanisms and industrial application. *The International Journal of Advanced Manufacturing Technology*, *37*(3-4), 265-278.

18. Jiang, Z., Lu, H., Wei, D., Linghu, K. Z., Zhao, X., Zhang, X., & Wu, D. (2014). Finite element method analysis of micro cross wedge rolling of metals. *Procedia Engineering*, *81*, 2463-2468.

19. Lu, H. N., Wei, D. B., Jiang, Z. Y., Wu, D., & Zhao, X. M. (2013, May). Study on the influence of temperature on the surface asperity in micro cross wedge rolling. In *AIP Conference Proceedings* (Vol. 1532, No. 1, pp. 1032-1037). AIP.

20. Qu, F., Jiang, Z., & Lu, H. (2016). Analysis of micro flexible rolling with consideration of material heterogeneity. *International Journal of Mechanical Sciences*, *105*, 182-190.

21. Engler, O., Schäfer, C., Brinkman, H. J., Brecht, J., Beiter, P., & Nijhof, K. (2016). Flexible rolling of aluminium alloy sheet—Process optimization and control of materials properties. *Journal of Materials Processing Technology*, *229*, 139-148.

22. Molotnikov, A., Lapovok, R., Gu, C. F., Davies, C. H. J., & Estrin, Y. (2012). Size effects in micro cup drawing. *Materials Science and Engineering: A*, *550*, 312-319.

23. Luo, L., Jiang, Z., Wei, D., Manabe, K. I., Zhao, X., Wu, D., & Furushima, T. (2016). Effects of surface roughness on micro deep drawing of circular cups with consideration of size effects. *Finite Elements in Analysis and Design*, *111*, 46-55.

24. Wang, G. C., Zheng, W., Wu, T., Jiang, H., Zhao, G. Q., Wei, D. B., & Jiang, Z. Y. (2012). A multi-region model for numerical simulation of micro bulk forming. *Journal of Materials Processing Technology*, *212*(3), 678-684.

25. Hu, Z. (2011). Realisation and application of size dependent FEM-simulation for deep drawing of rectangular work pieces. *CIRP Journal of Manufacturing Science and Technology*, *4*(1), 90-95.

26. Ma, N., & Dong, X. H. (2007). The size effects on process design of micro deep drawing. *Journal of Shanghai Jiaotong University (Science)*, *12*(3), 323-327.

27. Luo, L., Wei, D., Wang, X., Zhou, C., Huang, Q., Xu, J., ... & Jiang, Z. (2017). Effects of hydraulic pressure on wrinkling and earing in micro hydro deep drawing of SUS304 circular cups. *The International Journal of Advanced Manufacturing Technology*, *90*(1-4), 189-197.

28. Fang, Z., Jiang, Z., Wei, D., & Liu, X. (2015). Study on springback in micro V-bending with consideration of grain heterogeneity. *The International Journal of Advanced Manufacturing Technology*, *78*(5-8), 1075-1085.

29. Fan, Z., Wu, Y., Zhao, X., & Lu, Y. (2004). Simulation of polycrystalline structure with Voronoi diagram in Laguerre geometry based on random closed packing of spheres. *Computational materials science*, *29*(3), 301-308.

30. Gau, J. T., Principe, C., & Yu, M. (2007). Springback behavior of brass in micro sheet forming. *Journal of materials processing technology*, *191*(1-3), 7-10.

31. Ghazvinian, E., Diederichs, M. S., & Quey, R. (2014). 3D random Voronoi grain-based models for simulation of brittle rock damage and fabric-guided micro-fracturing. *Journal of Rock Mechanics and Geotechnical Engineering*, *6*(6), 506-521.

32. Dunand, M., Maertens, A. P., Luo, M., & Mohr, D. (2012). Experiments and modeling of anisotropic aluminum extrusions under multi-axial loading–Part I: Plasticity. *International Journal of Plasticity*, *36*, 34-49.

33. Luo, M., Dunand, M., & Mohr, D. (2012). Experiments and modeling of anisotropic aluminum extrusions under multi-axial loading–Part II: Ductile fracture. *International Journal of Plasticity*, *32*, 36-58.

34. Guan, Y., Pourboghrat, F., & Barlat, F. (2006). Finite element modeling of tube hydroforming of polycrystalline aluminum alloy extrusions. *International Journal of Plasticity*, *22*(12), 2366-2393.

35. Rousselier, G., Luo, M., & Mohr, D. (2012). Macroscopic plasticity modeling of anisotropic aluminum extrusions using a Reduced Texture Methodology. *International Journal of Plasticity*, *30*, 144-165.

36. Cao, J., Krishnan, N., Wang, Z., Lu, H., Liu, W. K., & Swanson, A. (2004). Microforming: experimental investigation of the extrusion process for micropins and its numerical simulation using RKEM. *Journal of Manufacturing Science and Engineering*, *126*(4), 642-652.

37. Shao, Y., Tang, T., Li, D., Tang, W., & Peng, Y. (2015). Crystal plasticity finite element modelling of the extrusion texture of a magnesium alloy. *Modelling and Simulation in Materials Science and Engineering*, *23*(5), 055011.

38. Mayama, T., Noda, M., Chiba, R., & Kuroda, M. (2011). Crystal plasticity analysis of texture development in magnesium alloy during extrusion. *International Journal of Plasticity*, *27*(12), 1916-1935.

39. Jiang, C. P., & Huang, Z. H. (2015). Finite Element Modeling of Grain Size Effect on the Mechanical Properties and Deformability of Titanium Alloy in Equal Channel Angular Pressure. In *Key Engineering Materials* (Vol. 661, pp. 91-97). Trans Tech Publications.

40. Sanusi, K., & Oosthuizen, G. (2016). Finite element modelling of the effects of average grain size and misorientation angle on the deformation. *The International Journal of Multiphysics, 5*(3)

41. Kathirgamanathan, P., & Neitzert, T. (2006). Modelling of metal extrusion using ABAQUS. In *The Proceedings of 3rd NZ Metals Industry Conference*.

42. Kroner, E. (1961). On the plastic deformation of polycrystals. *Acta Metallurgica*, *9*(2), 155-161.

43. R. Hill, J.R. Rice, Constitutive analysis of elastic-plastic crystals at arbitrary strain, J. Mech. Phys. Solids 20 (1972) 401-413.

44. Peirce, D., Asaro, R. J., & Needleman, A. (1982). An analysis of nonuniform and localized deformation in ductile single crystals. *Acta metallurgica*, *30*(6), 1087-1119.

45. Asaro, R. J., & Needleman, A. (1985). Overview no. 42 texture development and strain hardening in rate dependent polycrystals. *Acta metallurgica*, *33*(6), 923-953.

46. Kröner, E. (1981). Continuum theory of defects. *Physics of defects*, *35*, 217-315.

47. Kröner, E. (1959). Allgemeine kontinuumstheorie der versetzungen und eigenspannungen. *Archive for Rational Mechanics and Analysis*, *4*(1), 273.

48. Metals Handbook, Vol.2 - Properties and Selection: Nonferrous Alloys and Special-Purpose Materials, ASM International 10th Ed. 1990.

49. Quey, R., Dawson, P. R., & Barbe, F. (2011). Large-scale 3D random polycrystals for the finite element method: Generation, meshing and remeshing. *Computer Methods in Applied Mechanics and Engineering*, *200*(17-20), 1729-1745.

50. Quey, R., & Renversade, L. (2018). Optimal polyhedral description of 3D polycrystals: method and application to statistical and synchrotron X-ray diffraction data. *Computer Methods in Applied Mechanics and Engineering*, *330*, 308-333.

51. Quey, R., Villani, A., & Maurice, C. (2018). Nearly uniform sampling of crystal orientations. *Journal of Applied Crystallography*, *51*(4).

52. Krishnan, N., Cao, J., & Dohda, K. (2007). Study of the size effect on friction conditions in microextrusion—part I: microextrusion experiments and analysis. *Journal of Manufacturing Science and Engineering*, *129*(4), 669-676.

53. Kumar, V. S., Viswanathan, D., & Natarajan, S. (2006). Theoretical prediction and FEM analysis of superplastic forming of AA7475 aluminum alloy in a hemispherical die. *Journal of Materials Processing Technology*, *173*(3), 247-251.

Appendix

A.1 Python script to create section and to assign properties

A python script is given below to assign material heterogeneity to 75 grains.

```
from part import *
from material import *
from section import *
from assembly import *
mdb.models['Model-1'].HomogeneousSolidSection(material='avg', name='avg'
    , thickness=None)
mdb.models['Model-1'].HomogeneousSolidSection(material='plus_1', name='plus_1'
    , thickness=None)
mdb.models['Model-1'].HomogeneousSolidSection(material='plus_2', name='plus_2'
    , thickness=None)
mdb.models['Model-1'].HomogeneousSolidSection(material='plus_3', name=
    'plus_3', thickness=None)
mdb.models['Model-1'].HomogeneousSolidSection(material='minus_1', name=
    'minus_1', thickness=None)
mdb.models['Model-1'].HomogeneousSolidSection(material='minus_2', name=
    'minus_2', thickness=None)
mdb.models['Model-1'].HomogeneousSolidSection(material='minus_3', name=
    'minus_3', thickness=None)
```

```
for i in range (1,18):
        mdb.models['Model-1'].parts['TESS'].SectionAssignment(offset=0.0, offsetField=
    '', offsetType=MIDDLE_SURFACE, region=
    mdb.models['Model-1'].parts['TESS'].sets['POLY'+str(i)], sectionName='avg',
    thicknessAssignment=FROM_SECTION)

for i in range (18,31):
        mdb.models['Model-1'].parts['TESS'].SectionAssignment(offset=0.0, offsetField=
    '', offsetType=MIDDLE_SURFACE, region=
    mdb.models['Model-1'].parts['TESS'].sets['POLY'+str(i)], sectionName='plus_1',
    thicknessAssignment=FROM_SECTION)
for i in range (31,44):
        mdb.models['Model-1'].parts['TESS'].SectionAssignment(offset=0.0, offsetField=
    '', offsetType=MIDDLE_SURFACE, region=
    mdb.models['Model-1'].parts['TESS'].sets['POLY'+str(i)], sectionName='minus_1',
    thicknessAssignment=FROM_SECTION)
for i in range (44,54):
        mdb.models['Model-1'].parts['TESS'].SectionAssignment(offset=0.0, offsetField=
    '', offsetType=MIDDLE_SURFACE, region=
    mdb.models['Model-1'].parts['TESS'].sets['POLY'+str(i)], sectionName='plus_2',
    thicknessAssignment=FROM_SECTION)
```

```
for i in range (54,64):
        mdb.models['Model-1'].parts['TESS'].SectionAssignment(offset=0.0, offsetField=
    '', offsetType=MIDDLE_SURFACE, region=
    mdb.models['Model-1'].parts['TESS'].sets['POLY'+str(i)], sectionName='minus_2',
    thicknessAssignment=FROM_SECTION)
for i in range (64,70):
        mdb.models['Model-1'].parts['TESS'].SectionAssignment(offset=0.0, offsetField=
    '', offsetType=MIDDLE_SURFACE, region=
    mdb.models['Model-1'].parts['TESS'].sets['POLY'+str(i)], sectionName='plus_3',
    thicknessAssignment=FROM_SECTION)

for i in range (70,76):
        mdb.models['Model-1'].parts['TESS'].SectionAssignment(offset=0.0, offsetField=
    '', offsetType=MIDDLE_SURFACE, region=
    mdb.models['Model-1'].parts['TESS'].sets['POLY'+str(i)], sectionName='minus_3',
    thicknessAssignment=FROM_SECTION)
```

VITA

The author was born in the southernmost district of Bangladesh, Satkhira and passed his early school in Satkhira and Khulna. He obtained his Bachelor's degree in Mechanical Engineering in 2015 at Bangladesh University of Engineering and Technology (BUET). After graduation, he joined Karnaphuli Fertilizer Company Ltd. (KAFCO), as a Maintenance Engineer. Later, he worked as an Assistant Engineer in Bangladesh-China Power Company Ltd. (BCPCL) until July 2017. He joined the University of New Orleans to pursue his Master of Science in Engineering with concentration in Mechanical Engineering degree in Fall-2017 semester.